Monthly Notices
of the
ROYAL ASTRONOMICAL SOCIETY

MNRAS **428,** 2628–2644 (2013) doi:10.1093/mnras/sts232

Secondary anisotropies in CMB, skew-spectra and Minkowski Functionals

Dipak Munshi,[1]⋆ Peter Coles[1] and Alan Heavens[2,3]

[1]*School of Physics and Astronomy, Cardiff University, Queen's Buildings, 5 The Parade, Cardiff CF24 3AA*
[2]*Imperial Centre for Inference and Cosmology, Blackett Laboratory, Prince Consort Road, London SW7 2AZ*
[3]*Scottish Universities Physics Alliance (SUPA), Institute for Astronomy, University of Edinburgh, Blackford Hill, Edinburgh EH9 3HJ*

Accepted 2012 October 16. Received 2012 October 16; in original form 2012 September 2

ABSTRACT

Secondary contributions to the anisotropy of the cosmic microwave background (CMB), such as the integrated Sachs–Wolfe (ISW) effect, the thermal Sunyaev–Zel'dovich (tSZ) effect, and the effect of gravitational lensing, have distinctive non-Gaussian signatures, and full descriptions therefore require information beyond that contained in their power spectra. The Minkowski Functionals (MF) are well-known as tools for quantifying any departure from Gaussianity and are affected by noise and other sources of confusion in a different way from the usual methods based on higher-order moments or polyspectra, thus providing complementary tools for CMB analysis and cross-validation of results. In this paper we use the recently introduced skew-spectra associated with the MFs to probe the topology of CMB maps to probe the secondary non-Gaussianity as a function of beam smoothing in order to separate various contributions. We devise estimators for these spectra in the presence of realistic observational masks and present expressions for their covariance as a function of instrumental noise. Specific results are derived for the mixed ISW-lensing and tSZ-lensing bispectra as well as contamination due to point sources for noise levels that correspond to the *Planck* (143 GHz channel) and Experimental Probe of Inflationary Cosmology (*EPIC*; 150 GHz channel) experiments. The cumulative signal-to-noise ratio (S/N) for one-point generalized skewness parameters can reach an order of $\mathcal{O}(10)$ for Planck and two orders of magnitude higher for*EPIC*, i.e. $\mathcal{O}(10^3)$. We also find that these three skew-spectra are correlated, having correlation coefficients $r \sim 0.5$–1.0; higher l modes are more strongly correlated. Although the values of S/N increase with decreasing noise, the triplets of skew-spectra that determine the MFs become more correlated; the S/N of lensing-induced skew-spectra are smaller compared to that of a frequency-cleaned tSZ map.

Key words: cosmic background radiation – cosmology: theory – large-scale structure of Universe.

1 INTRODUCTION

All-sky multi-frequency cosmic microwave background (CMB) missions, such as the completed *Wilkinson Microwave Anisotropy Probe* (*WMAP*),[1] ongoing *Planck*[2] and future (proposed) Experimental Probe of Inflationary Cosmology (*EPIC*) survey (Bock et al. 2008, 2009; Baumann et al. 2009) or the European Space Agency's Cosmic Origin Explorer [COrE, The COrE Collaboration (2012)], are major sources of information about the properties of the primordial density fluctuations that seeded the process of galaxy formation in the Universe as well as other key aspects of cosmological theory, including the global isotropy (Copi et al. 2007; Hanson & Lewis 2009; Hoftuft et al. 2009) and topology of the Universe (Luminet et al. 2003; Roukemia et al. 2004).

The study of non-Gaussianity in the CMB fluctuations can provide valuable and detailed information regarding the physics of the early Universe of the inflationary epoch. In the standard slow-roll paradigm, the scalar field responsible for inflation fluctuates with a minimal amount of self-interaction which ensures that any non-Gaussianity generated during the inflation through self-interaction is expected to be small [Salopek & Bond 1990, 1991; Falk et al. 1993; Gangui et al. 1994; Acquaviva et al. 2003; Maldacena 2003; see also Bartolo, Matarrese & Riotto (2006) for a review]. Variants of the simple inflationary model such as multiple scalar fields, features in the inflationary potential,

⋆ E-mail: dipak.munshi@astro.cf.ac.uk
[1] http://map.gsfc.nasa.gov/
[2] http://www.rssd.esa.int/index.php?project=Planck

non-adiabatic fluctuations, non-standard kinetic terms, warm inflation or deviations from Bunch–Davies vacuum can, however, all lead to a higher level of primordial non-Gaussianity (Chen 2010).

However, the detection of departure from Gaussianity in the CMB can be due to either primary or secondary effects (or both), as well as the mode-coupling effects of secondaries and gravitational lensing along the observer's light cone. Secondary anisotropies resulting from the formation of structure are known to dominate at smaller angular scales, are highly non-Gaussian in nature (Cooray & Hu 2000; Cooray 2001b; Verde & Spergel 2002) and are arguably as interesting as their primary counterpart. One of the prominent contributions to the secondary non-Gaussianity is due to the mode-coupling of weak gravitational lensing and sources of secondary contributions such as the thermal Sunyaev–Zel'dovich (tSZ) effect (Goldberg & Spergel 1999a,b; Cooray & Hu 2000). Although weak lensing of the CMB produces its own characteristic signature in the angular power spectrum, its detection has proved to be difficult using the CMB power spectrum alone. Non-Gaussianity imprinted by lensing into the primordial CMB has recently been detected (Das et al. 2011; van Engelen et al. 2012), although with *Planck* the situation is likely to improve. Nevertheless, cross-correlating CMB data with external tracers means lensing signals can be probed at the level of the mixed bispectrum. After the first unsuccessful attempt to cross-correlate *WMAP* against Sloan Digital Sky Survey, recent efforts by Smith, Zahn & Dore (2007) have found a clear signal of weak lensing of the CMB, by cross-correlating *WMAP* against The NRAO VLA sky survey. Their work also underlines the link between three-point statistical estimators and the estimators for weak lensing effects on CMB. The understanding of secondaries is not only important in their own right, but also from the perspective of their impact on estimation of cosmological parameters (Smidt et al. 2010).

The study of non-Gaussianity is usually primarily focused on the bispectrum, as this saturates the Cramér–Rao bound (Babich 2005; Kamionkowski, Smith & Heavens 2011) and is therefore in a sense optimal; however in practice it is difficult to probe the entire configuration dependence in harmonic space contained within the bispectrum using noisy data (Munshi & Heavens 2010). The cumulant correlators are multi-point correlators collapsed to encode two-point statistics. These were introduced in the context of analysing galaxy clustering by Szapudi & Szalay (1999), and were later found to be useful for analysing projected surveys such as the Automated Plate Measurement galaxy survey (Munshi, Melott & Coles 2000). Being two-point statistics they can be analysed in multipole space by defining an associated power spectrum. Recent studies by Cooray (2006) and Cooray, Li & Melchiorri (2008) have demonstrated their wider applicability including, e.g., in 21cm studies. In more recent studies the skew- and kurt-spectra were found to be useful for analysing temperature (Munshi & Heavens 2010) as well as polarization maps (Munshi et al. 2011b) from CMB experiments and in weak lensing studies (Munshi et al. 2011a,d).

In addition to studies involving lower-order multi-spectra, MFs have been extensively developed as a statistical tool for non-Gaussianity in a cosmological setting for both two-dimensional (2D; projected) and three-dimensional (3D; redshift) surveys. Analytic results are known certain properties of the MFs of a Gaussian random field making them suitable for identifying non-Gaussianity. Examples of such studies include CMB data (Schmalzing & Górski 1998; Novikov, Schmalzing & Mukhanov 2000; Hikage et al. 2008b; Natoli et al. 2010), weak lensing (Matsubara & Jain 2001; Sato et al. 2001; Taruya et al. 2002; Munshi et al. 2012b), large-scale structure (Gott, Mellot & Dickinson 1986; Coles 1988; Gott et al. 1989, 1990, 1992; Melott 1990; Moore et al. 1992; Canavezes et al. 1998; Sahni, Sathyaprakash & Shandarin 1998; Schmalzing & Diaferio 2000; Kerscher et al. 2001; Hikage et al. 2002, 2008a; Park et al. 2005; Hikage, Komatsu & Mastubara 2006), 21 cm (Gleser et al. 2006), frequency-cleaned Sunyaev–Zel'dovich (SZ) maps (Munshi et al. 2012a) and *N*-body simulations (Schmalzing & Diaferio 2000; Kerscher et al. 2001). The MFs are spatially defined topological statistics and, by definition, contain statistical information of all orders in the moments. This makes them complementary to the poly-spectra methods that are defined in Fourier space (Munshi et al. 2011c). It is also possible that the two approaches will be sensitive to different aspects of non-Gaussianity and systematic effects although in the weakly non-Gaussian limit it has been shown that the MFs reduce to a weighted probe of the bispectrum (Hikage et al. 2006).

The skew-spectrum is a weighted statistic that can be tuned to a particular form of non-Gaussianity, such as that which may arise either during inflation at an early stage or from structure formation at a later time. The skew-spectrum retains more information about the specific form of non-Gaussianity than the (one-point) skewness parameter alone. This allows not only the exploration of primary and secondary non-Gaussianity but also the residuals from galactic foreground and unresolved point sources (PS). The skew-spectrum is directly related to the lowest order cumulant correlator and is also known as the two-to-one spectra in the literature (Cooray 2001a). In a series of recent publications the concept of skew-spectra was generalized to analyse the morphological properties of cosmological data sets or in particular the MFs by Munshi, Smidt & Cooray (2010), Munshi et al. (2012a,b), Pratten & Munshi (2012). The first of these three spectra, in the context of secondary-lensing correlation studies, was introduced by Munshi et al. (2011c) and was subsequently used to analyse data release from *WMAP* by Calabrese et al. (2010).

The primary aim of this paper is to consider the entire set of generalized skew-spectra resulting from the mode-coupling of secondary anisotropies and lensing of the CMB and the contribution thereof to non-Gaussian morphology of the CMB maps. We will be considering three different secondary-lensing correlation bispectra. The secondaries that we consider are the integrated Sachs–Wolfe (ISW) effect that dominates at large angular scales (Cooray 2002) and the tSZ effect that dominates at smaller angular scales (Birkinshaw 1999). In addition, we consider a foreground, namely the contribution from unresolved PSs. We will consider two experimental setups, the ongoing *Planck* satellite and the proposed *EPIC* satellite mission discussed above.

The layout of the paper is as follows. In Section 2 we briefly outline the bispectrum corresponding to lensing-secondary mode-coupling. Next, in Section 3, we review the formalism underlying the Minkowski Functionals, and in Section 4 we introduce the generalized skew-spectra associated with the MFs. In Section 5 we present the estimators for these spectra and their covariances. Finally, in Section 7 we discuss our results and comment on future implementation.

Throughout we will use the parameters of a *WMAP* cosmology (Larson et al. 2011).

2 MODE-COUPLING INDUCED BY LENSING-SECONDARY CROSS-CORRELATION AND THE RESULTING BISPECTRUM

The bispectrum of primary anisotropies encodes information that can be used to constrain the inflationary dynamics but, as discussed in the previous section, the primary contribution to non-Gaussianity is expected to be negligible in the simplest realizations of the generic inflationary scenario.

The secondary bispectrum provides valuable information regarding the low-redshift Universe and constrains structure formation scenarios. The secondaries can be broadly divided into three different types.

(i) *Gravitational* secondaries, caused by evolution in the gravitational potential along the observer's past light cone including the well-known ISW effect (Kofman & Starobinsky 1985; Martinez-Gonzaléz, Sanz & Silk 1990; Mukhanov, Feldman & Bandenberger 1992; Kaminkowski & Spergel 1994; Munshi, Souradeep & Starobinsky 1995; Mollerach et al. 1995; Boughn & Crittenden 2004) as well as the Rees–Sciama (RS) effect.

(ii) *Scattering* secondaries, such as the tSZ effect (Birkinshaw 1999), kinetic Sunyaev–Zel'dovich (kSZ) effect and the Ostriker–Vishniac effect (see e.g. Castro et al. 2004). These effects are caused by the interaction of the CMB photons with the intervening free-electron population.

(iii) *Lensing* secondaries caused by the propagation of photons through large scale structures.

Contributions to secondary bispectra can also arise from terms involving the cross-correlation of gravitational lensing and the effects of intervening material, such as the tSZ effect due to inverse-Compton scattering of CMB photons from hot gas in the intervening clusters. The decay of the peculiar gravitational potential along the line of sight in ΛCDM cosmology, introduced above as the ISW effect, is correlated to the lensing due to the potential, and can also generate an additional contribution to the secondary bispectrum in a similar fashion [see e.g. Cooray & Seth (2002) for a detailed discussion of various secondaries in the context of halo model]. The contribution to secondaries due to reionization of the Universe is detailed in Hu, Scott & Silk (1994). Foregrounds, such as unresolved PSs, can also contribute to the secondary bispectrum through their cross-correlation with the lensing of CMB.

On a different note, we comment that while the study of secondary anisotropies is important in their own right, they are also important in their effect on the calculation of error covariances in cosmological parameter estimation (Joudaki et al. 2010). Understanding the detailed statistical properties of secondary anisotropies like those we discuss here is therefore of utmost importance in the era of precision cosmology.

We will be dealing with the secondary bispectra involving the lensing of both primary anisotropies and other secondaries. Following Goldberg & Spergel (1999a,b) and Cooray & Hu (2000) we start by expanding the observed temperature anisotropy in terms of the primary contribution $\Theta_{\rm P}(\hat{\Omega})$, the secondary contribution $\Theta_{\rm S}(\hat{\Omega})$ and lensing of the primary $\Theta_{\rm L}(\hat{\Omega})$:

$$\Theta(\hat{\Omega}) = \Theta_{\rm P}(\hat{\Omega}) + \Theta_{\rm L}(\hat{\Omega}) + \Theta_{\rm S}(\hat{\Omega}) + \cdots \tag{1}$$

Here $\hat{\Omega} = (\theta, \phi)$ is the angular position on the surface of the sky. Expanding the respective contribution in terms of spherical harmonics $Y_{lm}(\hat{\Omega})$ we can write

$$\Theta_{\rm P}(\hat{\Omega}) \equiv \sum_{lm} (\Theta_{\rm p})_{lm} Y_{lm}(\hat{\Omega}); \quad \Theta_{\rm L}(\hat{\Omega}) \equiv \sum_{lm} [\nabla\psi(\hat{\Omega}) \cdot \nabla\Theta_{\rm P}(\hat{\Omega})]_{lm} Y_{lm}(\hat{\Omega}); \quad \Theta_{\rm S}(\hat{\Omega}) \equiv \sum_{lm} (\Theta_{\rm S})_{lm} Y_{lm}(\hat{\Omega}). \tag{2}$$

Here $\psi(\hat{\Omega})$ is the projected lensing potential (Goldberg & Spergel 1999a,b). The secondary bispectrum for the CMB takes contributions from products of P, L and S terms with varying order. The bispectrum $B^{\rm PLS}_{l_1 l_2 l_3}$ is defined as follows [see Bartolo et al. (2004) for generic discussion on the bispectrum and its symmetry properties]:

$$\begin{aligned} B^{\rm PLS}_{l_1 l_2 l_3} &\equiv \sum_{m_1 m_2 m_3} \begin{pmatrix} l_1 & l_2 & l_3 \\ m_1 & m_2 & m_3 \end{pmatrix} \int \langle \Theta_{\rm P}(\hat{\Omega}_1)\Theta_{\rm L}(\hat{\Omega}_2)\Theta_{\rm S}(\hat{\Omega}_3)\rangle Y^*_{l_1 m_1}(\hat{\Omega}_1) Y^*_{l_2 m_2}(\hat{\Omega}_2) Y^*_{l_3 m_3}(\hat{\Omega}_3) {\rm d}\hat{\Omega}_1\, {\rm d}\hat{\Omega}_2\, {\rm d}\hat{\Omega}_3; \\ &\equiv \sum_{m_1 m_2 m_3} \begin{pmatrix} l_1 & l_2 & l_3 \\ m_1 & m_2 & m_3 \end{pmatrix} \langle (\Theta_{\rm P})_{l_1 m_1} (\Theta_{\rm L})_{l_2 m_2} (\Theta_{\rm S})_{l_3 m_3} \rangle. \end{aligned} \tag{3}$$

The angular brackets represent *ensemble* averages. The matrices denote 3*j* symbols (Edmonds 1968) and the asterisks denote complex conjugation. It is possible to invert the relation assuming isotropy of the background Universe:

$$\langle (\Theta_{\rm P})_{l_1 m_1} (\Theta_{\rm L})_{l_2 m_2} (\Theta_{\rm S})_{l_3 m_3} \rangle = \begin{pmatrix} l_1 & l_2 & l_3 \\ m_1 & m_2 & m_3 \end{pmatrix} B^{\rm PLS}_{l_1 l_2 l_3}. \tag{4}$$

Finally the bispectrum $B^{\rm PLS}_{l_1 l_2 l_3}$ is expressed in terms of the un-lensed primary power spectrum $\mathcal{C}_l = \langle (\Theta_{\rm P})_{lm} (\Theta^*_{\rm P})_{lm} \rangle$ and the cross-spectra β_l (to be defined below) as follows:

$$B^{\rm PLS}_{l_1 l_2 l_3} = -\left\{ \beta_{l_3} \mathcal{C}_{l_1} \frac{l_2(l_2+1) - l_1(l_1+1) - l_3(l_3+1)}{2} + {\rm cyc.perm.} \right\} I_{l_1 l_2 l_3} \equiv \mathcal{B}_{l_1 l_2 l_3} I_{l_1 l_2 l_3}; \tag{5}$$

$$I_{l_1 l_2 l_3} \equiv \sqrt{\frac{(2l_1+1)(2l_2+1)(2l_3+1)}{4\pi}} \begin{pmatrix} l_1 & l_2 & l_3 \\ 0 & 0 & 0 \end{pmatrix} \tag{6}$$

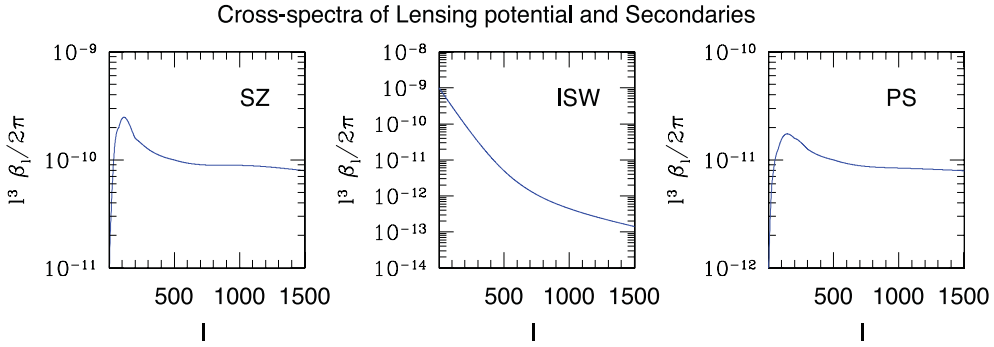

Figure 1. The cross-spectra β_l for various secondaries and lensing are plotted as a function of the harmonics l. From left to right, different panels correspond to cross-correlation of lensing potential and SZ, ISW and PS contribution. The cross-spectra β_l is being used in equation (5) for the construction of mixed bispectrum $B^{\rm PLS}_{l_1 l_2 l_3}$. It is defined in equation (7). Various estimators for the skew-spectra that we will use, associated with the three MFs, will be defined using the mixed bispectra. A background Λ cold dark matter (ΛCDM) cosmology is assumed. The details of these calculations, which rely on halo model prescriptions, can be found in Cooray (2001a).

[see Goldberg & Spergel (1999a,b) for a derivation]. The reduced bispectrum above is denoted as $\mathcal{B}_{l_1 l_2 l_3}$. To simplify the notation for the rest of this paper, we henceforth drop the superscript PLS form the bispectrum $B_{l_1 l_2 l_3}$. The cross-spectrum β_l introduced above represents the cross-correlation between the projected lensing potential $\psi(\hat{\Omega})$ and the secondary contribution $\Theta_{\rm S}(\hat{\Omega})$:

$$\langle \psi(\hat{\Omega})\Theta_{\rm S}(\hat{\Omega}')\rangle = \frac{1}{4\pi}\sum_{l=2}^{l_{\rm max}}(2l+1)\beta_l P_l(\hat{\Omega}\cdot\hat{\Omega}'). \tag{7}$$

The cross-spectra β_l take different forms for ISW-lensing, RS-lensing or SZ-lensing correlation and we assume a zero primordial non-Gaussianity. The reduced bispectrum $\mathcal{B}_{l_1 l_2 l_3}$ defined above using the notation $I_{l_1 l_2 l_3}$ is useful in separating the angular dependence from the dependence on power spectra C_l and β_l. We will use this to express the topological properties of the CMB maps. The β_l parameters for lensing-secondary correlations are displayed in Fig. 1. The left-, middle and right-hand panels in Fig. 1 displays SZ-lensing, ISW-lensing and PS lensing correlations. These results are based on halo model calculations performed using the halo model (Cooray 2001a).

The beam $b_l(\theta_b)$ and the noise of a specific experiment are characterized by the parameters $\sigma_{\rm beam}$ and $\sigma_{\rm rms}$:

$$b_l(\theta_b) = \exp\left[-l(l+1)\sigma^2_{\rm beam}\right];\quad \sigma_{\rm beam} = \frac{\theta_b}{\sqrt{8\ln(2)}}\quad n_l = \sigma^2_{\rm rms}\Omega_{\rm pix};\quad \Omega_{\rm pix} = \frac{4\pi}{N_{\rm pix}}, \tag{8}$$

where $\sigma_{\rm rms}$ is the rms noise per pixel that depends on the full width at half maxima or FWHM of the beam θ_b. The number of pixels $N_{\rm pix}$ required to cover the sky determines the size of the pixels $\Omega_{\rm pix}$. To incorporate the effect of experimental noise and the beam we have to replace $\mathcal{C}_l \rightarrow \mathcal{C}_l b_l^2(\theta_b) + n_l$, and the normalization of the skew-spectra that we will introduce later will be affected by the experimental beam and noise. The computation of scatter will also depend on these parameters. We will consider two different experimental setups: *Planck* and *EPIC*. The parameters of these experiments are tabulated in Table 1.

The optimal estimators for lensing-secondary mode-coupling bispectrum have been recently discussed by Munshi et al. (2011c). The estimators that we propose here are relevant in the context of constructing the MFs.

3 MINKOWSKI FUNCTIONALS

Integral geometry provides a natural framework within which to define the set of morphological descriptors for a random field. These descriptors are intrinsically defined in the spatial domain where they take into account all N-point correlators up to arbitrary order. Hadwiger's characterization theorem shows that a linear combination of these $d+1$ functionals will provide a complete morphological description of the morphology of d-dimensional objects [see Hadwiger (1959) for a formal treatment]. These functionals are more commonly referred to as the Minkowski Functionals. The Minkowski Functionals are usually calculated using volume-weighted curvature integrals for which the analytical results for a Gaussian random field are known (Adler 1981; Tomita 1986; Gott et al. 1990). More recently, the analytical values for weakly non-Gaussian fields have been calculated as a function of skewness parameters by using a perturbative approach based on the

Table 1 Parameters used to compute the skew-spectra and the associated scatter for the two different experiments, ongoing *Planck* (Planck Collaboration 2008) and *EPIC* (Baumann et al. 2009).

Mission	θ_b	$\sigma_{\rm pix}$	$\Omega_{\rm pix}$	Frequency
Planck	7.1 arcmin	2.2×10^{-6}	0.0349	143 (GHz)
EPIC	5.0 arcmin	8.0×10^{-9}	0.002	150 (GHz)

Edgeworth expansion (Matsubara 1994, 1995, 2003a; Matsubara & Yokohama 1996; Hikage et al. 2006). This approach allows us to use the MFs as a test of non-Gaussianity in the weakly perturbed regime as constrained by observation and predicted by models for inflation.

In two dimensions the MFs $V_0(\nu)$, $V_1(\nu)$ and $V_2(\nu)$ correspond, respectively, to the area of a set Σ, length of the perimeter of the set and the integrated curvature along its boundary. The MF $V_2(\nu)$ can be related to the well-known genus g and the Euler characteristic χ:

$$V_0(\nu) = \int_\Sigma \mathrm{d}a; \quad V_1(\nu) = \frac{1}{4}\int_{\partial\Sigma} \mathrm{d}l; \quad V_2(\nu) = \frac{1}{2\pi}\int_{\partial\Sigma} \kappa \mathrm{d}l. \tag{9}$$

Here $\mathrm{d}l$ and $\mathrm{d}a$ represent the length and surface element, respectively. In our analysis we consider a smoothed random field $\Theta(\hat{\Omega})$ with mean $\langle\Theta(\hat{\Omega})\rangle = 0$ and variance $\sigma_0^2(\theta_b) = \langle\Theta^2(\hat{\Omega})\rangle$. For a generic 2D weakly non-Gaussian random field Θ on the surface of the sky, the spherical harmonic decomposition using $Y_{lm}(\hat{\Omega})$ as basis functions $\Theta(\hat{\Omega}) = \sum_{lm}\Theta_{lm}Y_{lm}(\hat{\Omega})$ can be used to define the power spectrum $\mathcal{C}_l$ which is sufficient to characterize an isotropic Gaussian field $\langle\Theta_{lm}\Theta^*_{l'm'}\rangle = \mathcal{C}_l\delta_{ll'}\delta_{mm'}$.

We will be studying the MFs defined over the surface of the celestial sphere but equivalent results can be obtained in 3D using a Fourier decomposition (Pratten & Munshi 2012). The MFs for a 3D random Gaussian field are well known and are given by Tomita's formula (Tomita 1986).

For a non-Gaussian field the higher-order statistics such as bi- or tri-spectrum can describe the resulting mode–mode coupling. Alternatively topological measures such as the MFs (including the Euler characteristic or genus) can be employed to quantify deviations from Gaussianity. Indeed, it can be shown that the information content in both descriptions is equivalent in that, at leading order, the MFs can be constructed completely from the knowledge of the bispectrum alone.

The notations and analytical results in this section are being kept generic; however they will be specialized to the case of CMB sky in subsequent discussions.

The MFs denoted as $V_k(\nu)$ for a threshold $\nu = \Theta/\sigma_0$, where $\sigma_0^2(\theta_b) = \langle\Theta^2\rangle$ are perturbatively expressed as

$$V_k(\nu) = \frac{1}{(2\pi)^{(k+1)/2}}\frac{\omega_2}{\omega_{2-k}\omega_k}\exp\left(-\frac{\nu^2}{2}\right)\left(\frac{\sigma_1}{\sqrt{2}\sigma_0}\right)^k\left[V_k^{(0)}(\nu) + V_k^{(1)}(\nu)\sigma_0(\theta_b) + V_k^{(2)}(\nu)\sigma_0^2(\theta_b) + V_k^{(3)}(\nu)\sigma_0^3(\theta_b) + \cdots\right] \tag{10}$$

$$V_k^{(1)}(\nu) = \left[\left\{\frac{1}{6}S^{(0)}(\theta_b)H_{k+2}(\nu) + \frac{k}{3}S^{(1)}(\theta_b)H_k(\nu) + \frac{k(k-1)}{6}S^{(2)}(\theta_b)H_{k-2}(\nu)\right\}\right] \tag{11}$$

$$\sigma_j^2(\theta_b) = \frac{1}{4\pi}\sum_l (2l+1)[l(l+1)]^j\mathcal{C}_l b_l^2(\theta_b). \tag{12}$$

The constant ω_k introduced above is the volume of the unit sphere in k dimensions. $w_k = \pi^{k/2}/\Gamma(k/2+1)$ in two-dimension we will only need $\omega_0 = 1$, $\omega_1 = 2$ and $\omega_2 = \pi$. Here Γ is the gamma function. The lowest-order Hermite polynomials $H_k(\nu)$ are listed below.

$$H_{-1}(\nu) = \sqrt{\frac{\pi}{2}}\exp\left(\frac{\nu^2}{2}\right)\mathrm{erfc}\left(\frac{\nu}{\sqrt{2}}\right); \quad H_0(\nu) = 1, \quad H_1(\nu) = \nu, \quad H_2(\nu) = \nu^2 - 1, \quad H_3(\nu) = \nu^3 - 3\nu, \quad H_4(\nu) = \nu^4 - 6\nu^2 + 3,$$
$$H_n(\nu) = (-1)^n\exp\left(\frac{\nu^2}{2}\right)\frac{d}{d\nu^n}\exp\left(-\frac{\nu^2}{2}\right). \tag{13}$$

The expression equation (10) consists of two distinct contributions. The part $V_k^{(0)}(\nu) = H_{k-1}(\nu)$ signifies the MFs for a Gaussian random field. The other corrective contributions $V_k^{i\neq 0}(\nu)$ represent the departure from the Gaussian statistics. The leading order contribution to non-Gaussianity is encapsulated in $V_k^{(1)}(\nu)$ and depends on three generalized skewness parameters $S^{(0)}(\theta_b)$, $S^{(1)}(\theta_b)$, $S^{(2)}(\theta_b)$ defined in equations (15)–(17). Various second-order moments $\sigma_j(\theta_b)$ defined in equation (12) appear in equations (10) and (11) and can be expressed in terms of the power spectra $\mathcal{C}_l$ and the observational beam $b_l(\theta_b)$, assumed Gaussian with a full width at half-maximum θ_b [see equation (8) for definition]. The moment $\sigma_0(\theta_b)$ is a special case which relates to the variance of the field. The quantities $\sigma_1(\theta_b)$, $\sigma_2(\theta_b)$ are natural generalization of this variance, putting greater weight on higher-order harmonics; the variances that appear most frequently henceforth are $\sigma_0^2(\theta_b) = \langle\Theta^2\rangle$ and $\sigma_1^2(\theta_b) = \langle(\nabla\Theta)^2\rangle$.

Real space expressions for the triplets of skewness $S^{(i)}(\theta_b)$ are given below. These are natural generalizations of the ordinary skewness $S^{(0)}(\theta_b)$ that is used in many cosmological studies. They are all cubic statistics but are constructed from different cubic combinations.

$$S^{(0)}(\theta_b) \equiv \frac{S^{(\Theta^3)}(\theta_b)}{\sigma_0^4(\theta_b)} = \frac{\langle\Theta^3\rangle}{\sigma_0^4(\theta_b)}; \quad S^{(1)}(\theta_b) \equiv -\frac{3}{4}\frac{S^{(\Theta^2\nabla^2\Theta)}(\theta_b)}{\sigma_0^2(\theta_b)\sigma_1^2(\theta_b)} = -\frac{3}{4}\frac{\langle\Theta^2\nabla^2\Theta\rangle}{\sigma_0^2(\theta_b)\sigma_1^2(\theta_b)}; \quad S^{(2)}(\theta_b) \equiv -3\frac{S^{(\nabla\Theta\cdot\nabla\Theta\nabla^2\Theta)}(\theta_b)}{\sigma_1^4(\theta_b)}$$
$$= -3\frac{\langle(\nabla\Theta)\,.\,(\nabla\Theta)(\nabla^2\Theta)\rangle}{\sigma_1^4(\theta_b)}. \tag{14}$$

Notice that knowledge of the $S^{(i)}(\theta_b)$ parameters completely specifies the $V_k^{(2)}(\nu)$ parameters which characterize the lowest order departure from Gaussianity. The expressions in the harmonic domain are more useful in the context of CMB studies where these skewness parameters can be recovered from a masked sky using analytical tools that are commonly used for power spectrum analysis. The skewness parameter

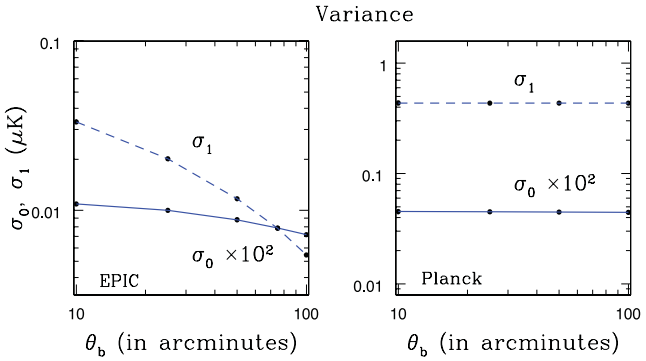

Figure 2. The variances $\sigma_0(\theta_b)$ and $\sigma_1(\theta_b)$, defined in equation (12), are plotted as a function of the FWHM θ_b. The left-hand panel corresponds to an experimental setup such as *EPIC* and the right-hand panel corresponds to *Planck*-type experiment. See Table 1 for detailed specifications regarding the noise level and beam.

$S^{(1)}(\theta_b)$ is constructed from the product field $[\Theta^2]$ and $[\nabla^2\Theta]$, whereas skewness parameter $S^{(2)}(\theta_b)$ relies on the combination of $[\nabla\Theta\cdot\nabla\Theta]$ and $[\nabla^2\Theta]$. By construction, the skewness parameter $S^{(2)}(\theta_b)$ has the highest weight for high l modes and $S_b^{(0)}$ has the lowest weight from high l modes.

The expressions in terms of the bispectrum $B_{l_1l_2l_3}$ [see equation (3) for definition] take the following form:

$$S^{(\Theta^3)}(\theta_b) = \frac{1}{4\pi}\sum_{l_i=2}^{l_{\max}} B_{l_1l_2l_3} I_{l_1l_2l_3} b_{l_1}(\theta_b) b_{l_2}(\theta_b) b_{l_3}(\theta_b), \tag{15}$$

$$S^{(\Theta^2\nabla^2\Theta)}(\theta_b) = -\frac{1}{12\pi}\sum_{l_i=2}^{l_{\max}} [l_1(l_1+1)+l_2(l_2+1)+l_3(l_3+1)] B_{l_1l_2l_3} I_{l_1l_2l_3} b_{l_1}(\theta_b) b_{l_2}(\theta_b) b_{l_3}(\theta_b), \tag{16}$$

$$S^{(\nabla\Theta\cdot\nabla\Theta\nabla^2\Theta)}(\theta_b) = \frac{1}{4\pi}\sum_{l_i=2}^{l_{\max}} [[l_1(l_1+1)+l_2(l_2+1)-l_3(l_3+1)]l_3(l_3+1)+\text{cyc.perm.}] B_{l_1l_2l_3} I_{l_1l_2l_3} b_{l_1}(\theta_b) b_{l_2}(\theta_b) b_{l_3}(\theta_b). \tag{17}$$

The dependence of the skew-spectra $S^{(i)}(\theta_b)$ and the beam $b_l(\theta_b)$ on the smoothing angular scale θ_b is being suppressed for brevity.

The angular bispectrum $B_{l_1l_2l_3}$ contains all the information at the level of the three-point angular correlation function. These results are generic and do not assume any specific form of non-Gaussianity. However, to arrive at specific expressions we will ignore the primordial non-Gaussianity, known to be sub-dominant, and concentrate on secondary non-Gaussianity. There is a family of one-point statistics, namely the well-known skewness parameters $S^{(i)}(\theta_b)$ introduced above, or pseudo-collapsed three-point function (Hinsaw et al. 1995), as well as the equilateral configuration statistics (Ferreira, Magueijo & Gorski 1998) which can all be expressed as linear combinations of the bispectrum terms. The generalized skewness parameters introduced above are also all linear combinations of the bispectrum weights but with varying weights. Using one-point statistics has the advantage of higher signal-to-noise ratio (S/N) but the price we pay is in terms of reduced power to discriminate individual contributions.

The series expansion for the MFs can be extended beyond the leading order at the level of the bispectrum to the next-to-leading order which involves the trispectrum of the temperature field. The lensing-induced trispectrum of the CMB will constitute the main next-to-leading order contribution. It is also important to realize that measurements of skewness parameters $S^{(0)}(\theta_b)$, $S^{(1)}(\theta_b)$ and $S^{(2)}(\theta_b)$ will not be independent but correlated with one another; the level of correlation depends on the noise and beam profile.

In Fig. 2 we have plotted the variance parameters $\sigma_0^2(\theta_b)$ and $\sigma_1^2(\theta_b)$ for various smoothing beams (assumed Gaussian). The four different FWHM that are considered are $\theta_b = 10$ arcmin, 25 arcmin, 50 arcmin and 100 arcmin, respectively. The parameter values only depend on the underlying CMB power spectra and the beam as well as the noise. They are used as normalization parameters while constructing the MFs from the generalized skewness parameters. Two different beam and noise levels are considered *EPIC* (left-hand panel) and *Planck* (right-hand panel). The one-point generalized skewness parameters are depicted in Fig. 3 for *Planck* and in Fig. 4 for *EPIC*. The background cosmology is that of ΛCDM.

In Fig. 4 the one-point skewness parameters $S^{(0)}(\theta_b)$, $S^{(1)}(\theta_b)$ and $S^{(2)}(\theta_b)$ (solid, short-dashed and long-dashed lines, respectively) are plotted as a function of smoothing scale θ_b. These parameters are defined in equation (14). The panels correspond to contributions from different types of secondary non-Gaussianity: cross-correlation of lensing and SZ effect (left-hand panel), cross-correlation of ISW and lensing (middle-panel); and cross-correlation of PS and lensing (right-hand panel). An experimental set up which is the same as *EPIC* was considered. See Table 1 for detailed specifications regarding the level of noise and beam. The bispectrum used in our calculation is given in equation (5) and the cross-spectra are plotted in Fig. 3; we plot the one-point skewness parameters for *Planck*.

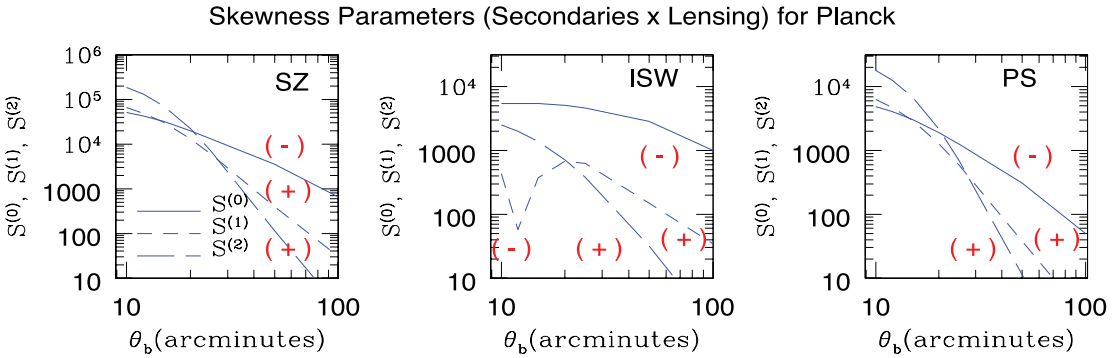

Figure 3. The absolute magnitudes of the one-point skewness parameters $S^{(0)}(\theta_b)$, $S^{(1)}(\theta_b)$ and $S^{(2)}(\theta_b)$ (solid, short-dashed and long-dashed lines, respectively) are plotted as a function of smoothing scale θ_b. These parameters are defined in equation (14). Various panels correspond to contributions from different types of secondary non-Gaussianity that represents the cross-correlation of lensing and SZ effect (left-hand panel), cross-correlation of ISW and lensing (middle panel), and cross-correlation of PSs and lensing (right-hand panel). The parameter $S^{(0)}(\theta_b)$ is negative for the entire range of FWHM or θ_b considered, for all three bispectra we have studied. The parameter $S^{(1)}(\theta_b)$ shows a transition from being negative to positive for the case of ISW bispectrum. All other skewness parameters stay positive as indicated. An experimental set up which is same as *Planck* was considered. See Table 1 for detailed specifications regarding the level of noise and beam. The bispectrum used in our calculation is given in equation (5) and the cross-spectra are plotted in Fig. 1.

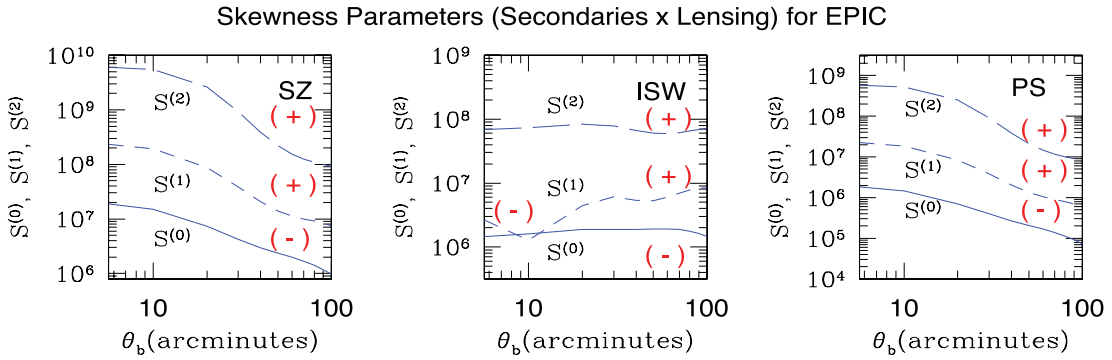

Figure 4. Same as the previous plot but for *EPIC*-type noise. The normalization of the skew-spectra depends on the noise level. The shape of the bispectrum is independent of the noise but depends on the experimental beam. Notice that $S^{(1)}(\theta_b)$ changes sign near $\theta_b \sim 10$ arcmin as before. $S^{(0)}(\theta_b)$ is negative for all three effects. The other parameters remain positive for the entire range of FWHM probed.

4 THE TRIPLETS OF SKEW-SPECTRA AND LOWEST ORDER CORRECTIONS TO GAUSSIAN MFS

The skew-spectrum has been studied previously in various cosmological contexts (Cooray 2001a), e.g. to estimate the bispectrum resulting from lensing-SZ correlation. The skew-spectra are cubic statistics constructed by cross-correlating two different fields. One of the fields used is a composite field (map) typically a product of two maps either in its original form or constructed by means of applying relevant differential operators. Examples of such derived maps that we will consider are $[\Theta^2(\hat{\Omega})]$, $[\nabla\Theta(\hat{\Omega})\cdot\nabla\Theta(\hat{\Omega})]$ and $[\nabla^2\Theta(\hat{\Omega})]$. The skew-spectra resulting from cross-correlating these maps are known as the *generalized* skew-spectra and are related to the three *generalized* skewness parameters introduced above. At the lowest order, the MFs themselves can be constructed using these generalized skewness parameters and contain equivalent information.

The detection of each individual mode of the primary or secondary bispectrum is still considered challenging. This is primarily due to the low S/N associated with each individual modes. All available information is therefore typically compressed into a single number – the skewness. This drastic data compression leads to a significant degradation of the power of the statistic to discriminate between models.

The first of the skew-spectra that we will study is the one introduced by Cooray (2001a) and later generalized by Munshi & Heavens (2010). It is related to sometimes known as the two-to-one power spectrum and is constructed by cross-correlating the squared map $[\Theta^2(\hat{\Omega})]$ with the original map $\Theta(\hat{\Omega})$. The second skew-spectrum is constructed by cross-correlating the squared map $[\Theta^2(\hat{\Omega})]$ with $[\nabla^2\Theta(\hat{\Omega})]$. Analogously the third skew-spectrum represents the cross-spectra that can be constructed using $[\nabla\Theta(\hat{\Omega})\cdot\nabla\Theta(\hat{\Omega})]$ and $[\nabla^2\Theta(\hat{\Omega})]$ maps.

$$S_l^{(0)}(\theta_b) \equiv \frac{1}{12\pi\sigma_0^4(\theta_b)} S_l^{(\Theta^2,\Theta)}(\theta_b) \equiv \frac{1}{12\pi\sigma_0^4(\theta_b)} \frac{1}{2l+1} \sum_m \mathrm{Real}([\Theta]_{lm}[\Theta^2]^*_{lm}) = \frac{1}{12\pi\sigma_0^4(\theta_b)} \sum_{l_1 l_2} B_{ll_1l_2} J_{ll_1l_2} b_l(\theta_b) b_{l_1}(\theta_b) b_{l_2}(\theta_b), \tag{18}$$

$$S_l^{(1)}(\theta_b) \equiv \frac{1}{16\pi\sigma_0^2(\theta_b)\sigma_1^2(\theta)} S_l^{(\Theta^2,\nabla^2\Theta)}(\theta_b) \equiv \frac{1}{16\pi\sigma_0^2(\theta_b)\sigma_1^2(\theta_b)} \frac{1}{2l+1} \sum_m \mathrm{Real}([\nabla^2\Theta]_{lm}[\Theta^2]^*_{lm})$$
$$= \frac{1}{16\pi\sigma_0^2(\theta_b)\sigma_1^2(\theta_b)} \sum_{l_i} [l(l+1)+l_1(l_1+1)+l_2(l_2+1)] B_{ll_1l_2} J_{ll_1l_2} b_{l_1}(\theta_b) b_{l_2}(\theta_b) b_{l_3}(\theta_b), \tag{19}$$

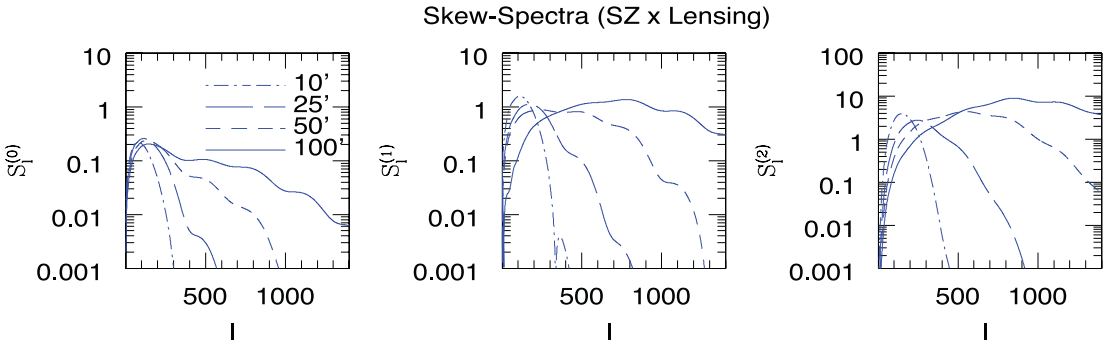

Figure 5. The three skew-spectra corresponding to the three MFs $S_l^{(0)}(\theta_b)$ (left-hand panel), $S_l^{(1)}(\theta_b)$ (middle panel) and $S_l^{(2)}(\theta_b)$ (right-hand panel) are plotted for the mixed secondary bispectrum of SZ×Lensing as a function of the harmonics l. A background ΛCDM cosmology is assumed. The skew-spectra are defined in equations (15), (16) and (17), respectively. All other sources of non-Gaussianity are ignored. Four different Gaussian-beams are considered. The curves from left to right correspond to $\theta_b = 10$, 25, 50, 100 arcmin in each panel. The normalization of the skew-spectra is somewhat arbitrary and do not affect the S/N. We have ignored the presence of noise, as defined in equation (12), in our calculation of $\sigma_0(\theta_b)$ and $\sigma_1(\theta_b)$, respectively. Notice that for a given θ_b higher-order skew-spectra peak at a higher l. The S/N of the skew-spectra associated with SZ effect are plotted in Fig. 8 for *Planck* and in Fig. 9 for *EPIC* noise level, respectively. The skew-spectra are not uncorrelated. The cross-correlation among various skew-spectra is displayed in Fig. 10 for *Planck* and in Fig. 11 for *EPIC*.

$$S_l^{(2)}(\theta_b) \equiv \frac{1}{8\pi\sigma_1^4(\theta_b)} S_l^{(\nabla\Theta\cdot\nabla\Theta,\nabla^2\Theta)}(\theta_b) \equiv \frac{1}{8\pi\sigma_1^4(\theta_b)} \frac{1}{2l+1} \sum_m \mathrm{Real}\left([\nabla\Theta\cdot\nabla\Theta]_{lm}[\nabla^2\Theta]^*_{lm}\right) u$$
$$= \frac{1}{8\pi\sigma_1^4(\theta_b)} \sum_{l_i} [[l(l+1)+l_1(l_1+1)-l_2(l_2+1)]l_2(l_2+1)+\mathrm{cyc.perm.}] B_{ll_1l_2} J_{ll_1l_2} b_l(\theta_b) b_{l_1}(\theta_b) b_{l_2}(\theta_b), \quad (20)$$

$$J_{l_1l_2l_3} \equiv \frac{I_{l_1l_2l_3}}{2l_3+1} = \sqrt{\frac{(2l_2+1)(2l_3+1)}{(2l_1+1)4\pi}} \begin{pmatrix} l_1 & l_2 & l_3 \\ 0 & 0 & 0 \end{pmatrix}, \quad (21)$$

$$S^{(i)}(\theta_b) = \sum_l (2l+1) S_l^{(i)}(\theta_b). \quad (22)$$

Each of these spectra probes the same bispectrum $B_{ll_1l_2}$ but with different weights. Each triplet of modes specifies a triangle in the harmonic domain and the skew-spectra sum over all possible configuration of the bispectrum keeping one of its sides l fixed.

In terms of the skew-spectra $S_l^{(k)}(\theta_0)$, we can now define a set of three power-spectra associated with the three MFs $[V_k^{(1)}(\nu)]_l$:

$$[V_k^{(1)}(\nu)]_l = \left[\left\{\frac{1}{6} S_l^{(0)}(\theta_b) H_{k+2}(\nu) + \frac{k}{3} S_l^{(1)}(\theta_b) H_k(\nu) + \frac{k(k-1)}{6} S_l^{(2)}(\theta_b) H_{k-2}(\nu)\right\}\right]; \qquad V_k^{(1)}(\nu) = \sum_l (2l+1)[V_k^{(1)}(\nu)]_l. \quad (23)$$

The extraction of skew-spectra from data is relatively straightforward. The procedure consists of the construction of the relevant maps in real space either by algebraic or by differential operations and then cross-correlating them in multipole space. Issues related to mask and noise will be dealt with in later sections. We will show that even in the presence of a mask the computed skew-spectra can be inverted to give an unbiased estimate of all-sky skew-spectra; the presence of noise will only affect the scatter. We have explicitly displayed the experimental beam b_l in all our expressions.

In Figs 5–7, we have presented the three different skew-spectra S_l as a function of the harmonics l. The skew-spectra for a generic bispectrum are defined in equations (18) and (19) and in equation (20). In Fig. 5 we present the skew-spectra corresponding to the SZ effect cross-correlated to lensing. The Fig. 6 we present the skew-spectra for the ISW effect and Fig. 7 shows the skew-spectra for unresolved PSs. The skew-spectra are sensitive to the beam $b_l(\theta_b)$; moreover the skew-spectra at a given l, i.e. $S_l^{(i)}(\theta_b)$, depend on the bispectrum $B_{l_1l_2l_3}$ defined over the entire range of modes specified by all possible l values that are being probed. The distinct shape of these individual spectra can be used to study the nature of their origin (i.e. primordial or secondary). Specific models of primary non-Gaussianity such as local or equilateral too will have distinct shapes for the $S_l^{(i)}(\theta_b)$ parameters though such contributions will be subdominant for currently allowed levels of primordial non-Gaussianity.

It is important to stress that these three skew-spectra do not contain completely independent information; the errors associated with them are correlated. We next turn to a detailed derivation of the S/N level of these estimators and the level of cross-correlation among these spectra for a given observational strategy. The derivations are accurate for near all-sky coverage; for more accurate modelling a computationally expensive but conceptually straightforward Monte Carlo analysis is required.

Using the estimator equation (18) previous studies have focused towards a detection of lensing-secondary correlation for individual *WMAP* frequency channels using raw as well as frequency-cleaned maps (Calabrese et al. 2010). These studies used the KQ75 mask and were

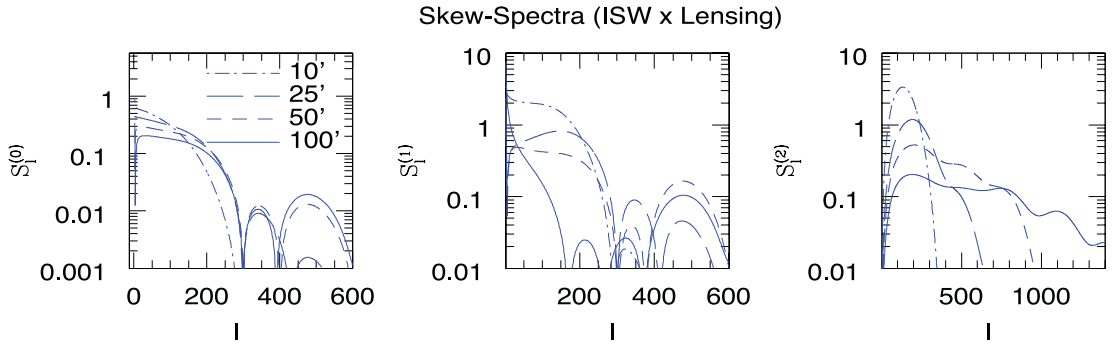

Figure 6. The skew-spectra $S_l^{(0)}(\theta_b)$, $S_l^{(1)}(\theta_b)$ and $S_l^{(2)}(\theta_b)$ for ISW × Lensing are plotted as a function of the harmonics l. Notice that skew-spectra corresponding to ISW are dominant at smaller ls while the ones corresponding to SZ dominate at larger l values. The skew-spectra, being integrated measures, depend on the entire harmonic range of the bispectra. The shape of the skew-spectra can play an important role in separating individual contributions of secondary non-Gaussianity.

limited by the *WMAP* resolution $N_{\rm side} = 512$ and an $l_{\rm max} = 600$. No significant evidence for a non-Gaussian signal from the lensing-secondary correlation was found in any of the individual bands, 2σ and 3σ evidence were obtained both for lensing-ISW and for lensing-SZ signals in the foreground-cleaned Q-band maps, respectively. They also found the PS amplitude at the bispectrum level to be consistent with previous measurements. With higher resolution maps available from *Planck* as well as other future missions such as *EPIC* it will be possible not only to achieve a cross-validation using multiple skew-spectra, but also to reconstruct the topological properties and compare them with the ones obtained in the pixel domain.

A great deal of attention has recently been focused on designing optimal estimators. Indeed this is true that for current generation of experiments (*WMAP*) the mere detection of non-Gaussianity remains a challenging task because of the low S/N. Optimality of an estimator may not be a crucial issue for high-resolution data from experiments such as *Planck*, at least for the detection of secondaries, as very high level of S/N is expected. Attention then will shift to the characterization of non-Gaussianity using an array of estimators to separate different components of non-Gaussianity (primordial and secondary) and provide the level of contamination from foregrounds such as PSs. The skew-spectra associated with MFs can play a valuable role in this direction. The main advantage of computing the skew-spectra being a direct estimator which can be computed using a pseudo-$\mathcal{C}_\ell$ (PCL) based approach, and the covariances can be characterized analytically even in the presence of an arbitrary mask and non-stationary noise.

5 ESTIMATOR, SKY COVERAGE AND ERROR ANALYSIS

The results derived above correspond to a situation in which an all-sky map is available which is free from noise. However, in reality we have to often deal with issues that are related to the presence of a mask and (possibly inhomogeneous) noise. Partial sky coverage introduces mode–mode coupling in the harmonic domain in such a way that individual masked harmonics become linear combinations of all-sky harmonics. The coefficients for this linear transformation depend on specific choice of mask through its own harmonic coefficients. We will devise a method that can be used to correct for this mode–mode coupling based on the PCL method devised by Hivon et al. (2002) for power spectrum analysis and later developed by Munshi et al. (2011c) for analysing the skew-spectra and the kurt-spectrum (Munshi et al. 2011b).

Consider two generic fields $A(\hat{\Omega})$ and $B(\hat{\Omega})$ and denote their harmonic decompositions in the presence of a mask $w(\hat{\Omega})$ as $\tilde{A}_{lm}$ and $\tilde{B}_{lm}$. Notice that the mask is completely general and our results do not depend on any specific symmetry requirements such as the azimuthal symmetry. The fields A and B may correspond to any of the fields we have considered above. In a generic situation A and B will denote

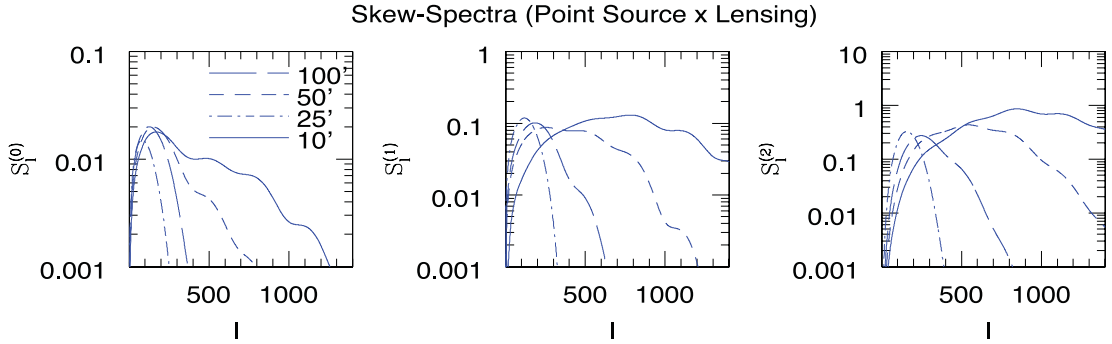

Figure 7. The skew-spectra $S_l^{(0)}(\theta_b)$, $S_l^{(1)}(\theta_b)$ and $S_l^{(2)}(\theta_b)$ for PS × Lensing are plotted as a function of the harmonics l. The similarity of the underlying bispectrum for unresolved PSs and the SZ effect means the shape of resulting skew-spectra is similar.

composite fields and the harmonics A_{lm} and B_{lm} will correspond to any of the harmonics listed in equation (22) i.e. $[\Theta^2]_{lm}$, $[\nabla\Theta\cdot\nabla\Theta]_{lm}$ and $[\nabla^2\Theta]_{lm}$:

$$\tilde{A}_{lm} = \int \mathrm{d}\hat{\Omega}\; Y^*_{lm}(\hat{\Omega})\,[w(\hat{\Omega})\,A(\hat{\Omega})]; \tag{24}$$

$$\tilde{A}_{lm} = \sum_{l_i m_i} (-1)^m\; I_{ll_1l_2} \begin{pmatrix} l_1 & l_2 & l \\ m_1 & m_2 & -m \end{pmatrix} w_{l_1m_1} A_{l_2m_2}. \tag{25}$$

Similar expressions hold for B. The above expression relates the masked harmonics denoted by $\tilde{A}_{lm}$ and $\tilde{B}_{lm}$ with their all-sky counterparts A_{lm} and B_{lm}, respectively. In their derivation we use the Gaunt integral to express the overlap integrals involving three spherical harmonics in terms of the $3j$ symbols (Edmonds 1968). The matrix $I_{l_1l_1l_3}$ encodes the overlap integral defined in equation (6). The expressions also depend on the harmonics of the mask w_{lm}. If we now denote the (cross) power spectrum constructed from the masked harmonics and denote it by $\tilde{S}_l(\theta_b)$ and its all-sky counterpart by $\hat{S}_l(\theta_b)$, we can write

$$\tilde{S}^{A,B}_l(\theta_b) = \frac{1}{2l+1}\sum_m \tilde{A}_{lm}\tilde{B}^*_{lm}; \quad \tilde{S}^{A,B}_l(\theta_b) = \sum_{l'} M_{ll'} S^{A,B}_l(\theta_b); \quad M_{ll'} = \frac{1}{2l+1}\sum_{l'l''} I^2_{ll'l''}|w_{l''}|^2; \tag{26}$$

$$\hat{S}^{A,B}_l(\theta_b) = \sum_{l'}[M^{-1}]_{ll'}\tilde{S}^{A,B}_{l'}(\theta_b); \quad \left\langle \delta\hat{S}^{A,B}_l(\theta_b)\delta\hat{S}^{A,B}_{l'}(\theta_b)\right\rangle = \sum_{LL'} M^{-1}_{lL}\left\langle \delta\tilde{S}^{A,B}_L(\theta_b)\delta\tilde{S}^{A,B}_{L'}(\theta_b)\right\rangle M^{-1}_{L'l'}; \quad \left\langle \hat{S}^{A,B}_l(\theta_b)\right\rangle = S^{A,B}_l(\theta_b); \tag{27}$$

$$\delta S^{A,B}_l(\theta_b) = \left\langle \hat{S}^{A,B}_{l'}(\theta_b)\right\rangle - S^{A,B}_l(\theta_b); \qquad \{A,B\} \in \left\{\Theta, \Theta^2, (\nabla\Theta\cdot\nabla\Theta), \nabla^2\Theta\right\}. \tag{28}$$

The final expressions will be independent of the azimuthal quantum number m due to our assumption of isotropy. In the above derivation we have used the orthogonality properties of the $3j$ symbols.

It is interesting to note that the *convolved* power spectrum estimated from the masked sky is a linear combination of all-sky spectra and depends only on the power spectrum of the mask used. The linear transform is encoded in the mode–mode coupling matrix $M_{ll'}$ which is constructed from the knowledge of the power spectrum of the mask. In certain situations where the sky coverage is very restricted the direct inversion of the mode-mixing matrix M may not be possible due to its singularity and binning may be essential. Based on these results it is possible to define an unbiased estimator that we denote by $\hat{S}^{A,B}_l(\theta_b)$. The noise, due to its Gaussian nature, does not contribute in these estimators which remains unbiased. However, the presence of noise is felt in the increase in the scatter or covariance of these estimators (which can be computed analytically). The symbol $S^{A,A}_l(\theta_b)$ denotes the power spectrum of the field $A(\hat{\Omega})$; $A(\hat{\Omega})$ is a generic field that is used for the construction of generalized skew-spectra. The derivation of the covariance depends on a Gaussian approximation, i.e. we ignore higher-order non-Gaussianity in the fields. $\mathcal{C}_l$ is the ordinary CMB power spectra; it also includes the effect of instrumental noise and beam $\mathcal{C}_l(\theta_b) = \mathcal{C}^S_l b^2_l(\theta_b) + n_l$. For a survey with homogeneous noise, we can write $\mathcal{C}^N_l = \Omega_{\rm p}\sigma^2_{\rm N}$ where $\Omega_{\rm p}$ is the pixel area and $\sigma_{\rm N}$ is the noise rms. In a regime when noise contributions dominate, the MFs can be approximated by a Gaussian approximation. The resulting expressions are listed below:

$$\left\langle \delta S^{A,B}_l(\theta_b)\delta S^{A,B}_{l'}(\theta_b)\right\rangle = \frac{1}{2l+1}\left[S^{A,A}_l(\theta_b)\; S^{B,B}_l(\theta_b) + [S^{A,B}_l(\theta_b)]^2\right]; \tag{29}$$

$$\left\langle \delta S^{A_1,B_1}_l(\theta_b)\delta S^{A_2,B_2}_{l'}(\theta_b)\right\rangle = \frac{1}{2l+1}\left[S^{A_1,A_2}_l(\theta_b)\; S^{B_1,B_2}_l(\theta_b) + S^{A_1,B_2}_l(\theta_b)\; S^{A_2,B_1}_l(\theta_b)\right]; \tag{30}$$

$$\{A_1, B_1, A_2, B_2\} \in \left\{\Theta, \Theta^2, (\nabla\Theta\cdot\nabla\Theta), \nabla^2\Theta\right\}. \tag{31}$$

In the next section we will provide detailed explicit expressions for various choices of estimators.

At this stage, we want to point out that equivalent relations, for the scatter in the power-spectra associated with MFs defined in equation (23), are easy to obtain. The convolved and deconvolved estimators for these power-spectra will be denoted by $[\tilde{V}^{(2)}_k]_l$ and $[\tilde{V}^{(2)}_k]_l$, respectively. These estimators and their scatters are related by the following expressions:

$$\left[\hat{V}^{(1)}_k\right]_l = \sum_{l'}[M^{-1}]_{ll'}\left[\tilde{V}^{(1)}_k\right]_l; \qquad \left\langle \delta\hat{V}^{(1)}_k\delta\hat{V}^{(1)}_{k'}\right\rangle = \sum_{LL'} M^{-1}_{lL}\left\langle \delta[\tilde{V}^{(1)}_k]_l\delta[\tilde{V}^{(1)}_{k'}]_{l'}\right\rangle M^{-1}_{L'l'}. \tag{32}$$

We have suppressed the argument ν in the above expressions. Expressions of scatters in $[V^{(2)}_k]_l$, i.e. $\delta[V^{(2)}_k]_l$, can be obtained in terms of the scatter in the skew-spectra $\delta S^{(i)}_l$ using equation (23):

$$\delta\left[\tilde{V}^{(2)}_k(\nu)\right]_l = \left[\left\{\frac{1}{6}\delta\tilde{S}^{(0)}_l(\theta_b)H_{k+2}(\nu) + \frac{k}{3}\delta\tilde{S}^{(1)}_l(\theta_b)H_k(\nu) + \frac{k(k-1)}{6}\delta\tilde{S}^{(2)}_l(\theta_b)H_{k-2}(\nu)\right\}\right]. \tag{33}$$

The two-to-one estimators are from a family of non-Gaussian estimators. The three-to-one estimator probes the four-point correlation function or equivalently the (angular) trispectrum $T^{l_1 l_2}_{l_3 l_4}(L)$ (Cooray et al. 2008). These spectra have been used to probe primordial non-Gaussianity beyond the lowest order, i.e. to separate contributions from $\tau_{\rm NL}$ and $g_{\rm NL}$. The two-to-two spectrum or the power spectrum of the squared CMB maps was found to be useful in the context of studies of weak lensing-induced CMB non-Gaussianity (Cooray & Kesden 2003). The next order corrections to the generalized skew-spectra too have been constructed using such an approach (Munshi et al. 2010) in the context of studies of MF. The PCL formalism discussed above is useful for constructing quadruplets of trispectra. The error estimates for these higher-order contributions too can be computed using a formalism we outline next.

6 EXPLICIT EXPRESSIONS FOR COVARIANCES

As we have already stressed, the estimators we have introduced for the skew-spectra are correlated and do not carry independent information. Their correlation structure depends on the experimental beam, noise and sky-coverage. Just as with non-Gaussianity, partial sky coverage also introduces mode–mode coupling. However, using the mode-mixing matrix defined in equation (26) it is possible to deconvolve the convolved skew-spectra $\tilde{S}_l$. In this section, we list the expressions for the co-variance of various estimators for skew-spectra. The variances or the scatter of the skew-spectra defined in equation (28) take the following forms:

$$\left\langle [\delta S_l^{\Theta^2,\Theta}(\theta_b)]^2 \right\rangle_c \equiv \left\langle [S_l^{\Theta^2,\Theta}(\theta_b)]^2 \right\rangle_c - \left\langle S_l^{\Theta^2,\Theta}(\theta_b) \right\rangle_c^2 = \frac{f_{\rm sky}^{-1}}{2l+1}\left[S_l^{\Theta^2,\Theta^2}(\theta_b)\; S_l^{\Theta,\Theta}(\theta_b) + [S_l^{\Theta^2,\Theta}(\theta_b)]^2 \right], \tag{34}$$

$$\left\langle [\delta S_l^{\Theta^2,\nabla^2\Theta}(\theta_b)]^2 \right\rangle_c \equiv \left\langle [S_l^{\Theta^2,\nabla^2\Theta}(\theta_b)]^2 \right\rangle_c - \left\langle S_l^{\Theta^2,\nabla^2\Theta}(\theta_b) \right\rangle_c^2 = \frac{f_{\rm sky}^{-1}}{2l+1}\left[S_l^{\Theta^2,\Theta^2}(\theta_b)\; S_l^{\nabla^2\Theta,\nabla^2\Theta}(\theta_b) + [S_l^{\Theta^2,\nabla^2\Theta}(\theta_b)]^2 \right], \tag{35}$$

$$\left\langle [\delta S_l^{\nabla^2\Theta,\nabla\Theta\cdot\nabla\Theta}(\theta_b)]^2 \right\rangle_c \equiv \left\langle [S_l^{\nabla^2\Theta,\nabla\Theta\cdot\nabla\Theta}(\theta_b)]^2 \right\rangle_c - \left\langle S_l^{\nabla^2\Theta,\nabla\Theta\cdot\nabla\Theta}(\theta_b) \right\rangle_c^2 = \frac{f_{\rm sky}^{-1}}{2l+1}\left[S_l^{\nabla^2\Theta,\nabla^2\Theta}(\theta_b)\; S_l^{\nabla\Theta\cdot\nabla\Theta,\nabla\Theta\cdot\nabla\Theta}(\theta_b) + [S_l^{\nabla^2\Theta,\nabla\Theta\cdot\nabla\Theta}(\theta_b)]^2 \right]. \tag{36}$$

Here $f_{\rm sky}$ is the fraction of the sky covered. The expressions for the cross-covariances can also be computed using the similar technique. We express the harmonics of the composite fields such as $[\Theta^2]_{lm}$, $[\nabla\Theta\cdot\nabla\Theta]_{lm}$ in terms of harmonics of the $[\Theta]_{lm}$ field using the overlap integral. The final equations are derived using Wick's theorem to simplify the resulting expressions.

$$\left\langle \delta S_l^{\Theta^2,\Theta}(\theta_b)\; \delta S_l^{\nabla\Theta\cdot\nabla\Theta,\Delta^2\Theta}(\theta_b) \right\rangle_c = \frac{f_{\rm sky}^{-1}}{2l+1}\left[[S_l^{\Theta^2,\nabla\Theta\cdot\nabla\Theta}(\theta_b)][S_l^{\Theta,\Delta^2\Theta}(\theta_b)] + [S_l^{\Theta,\nabla\Theta\cdot\nabla\Theta}(\theta_b)][S_l^{\Theta^2,\Delta^2\Theta}(\theta_b)] \right], \tag{37}$$

$$\left\langle \delta S_l^{\Theta^2,\Theta}(\theta_b)\; \delta S_l^{\Theta^2,\Delta^2\Theta}(\theta_b) \right\rangle_c = \frac{f_{\rm sky}^{-1}}{2l+1}\left[S_l^{\Theta^2,\Theta^2}(\theta_b)\; S_l^{\Theta,\Delta^2\Theta}(\theta_b) + S_l^{\Theta^2,\Theta}(\theta_b)\; S_l^{\Theta^2,\Delta^2\Theta}(\theta_b) \right], \tag{38}$$

$$\left\langle \delta S_l^{\nabla\Theta\cdot\nabla\Theta,\Delta^2\Theta}(\theta_b)\; \delta S_l^{\Theta^2,\Delta^2\Theta}(\theta_b) \right\rangle_c = \frac{f_{\rm sky}^{-1}}{2l+1}\left[S_l^{\Theta^2,\nabla\Theta\cdot\nabla\Theta}(\theta_b)\; S_l^{\Delta^2\Theta,\Delta^2\Theta}(\theta_b) + S_l^{\Theta^2,\Delta^2\Theta}(\theta_b) S_l^{\nabla\Theta\cdot\nabla\Theta,\Delta^2\Theta}(\theta_b) \right]. \tag{39}$$

The final expressions that we derive are applicable to near all-sky surveys. When a small portion of the sky is covered a sky patch version of our calculations can be performed using 2D Fourier analysis instead of the spherical harmonic analysis that we use here. Some of the terms appearing in these expressions can be expressed in terms of the bispectrum. If we assume that the instrumental noise is Gaussian then there is no contribution from noise in these expressions.

$$S_l^{\langle\Theta^2,\nabla^2\Theta\rangle}(\theta_b) = -\sum_{l_i=2}^{l_{\rm max}} l(l+1)\; B_{ll_1l_2} J_{ll_1l_2} b_l b_{l_1} b_{l_2}, \tag{40}$$

$$S_l^{\langle\Theta,\nabla\Theta\cdot\nabla\Theta\rangle}(\theta_b) = \sum_{l_i=2}^{l_{\rm max}} B_{ll_1l_2} J_{ll_1l_2}[l(l+1) + l_1(l_1+1) - l_2(l_2+1)] b_l b_{l_1} b_{l_2}, \tag{41}$$

$$S_l^{\langle\nabla\Theta\cdot\nabla\Theta,\Delta^2\Theta\rangle}(\theta_b) = -\sum_{l_i=2}^{l_{\rm max}} B_{ll_1l_2} J_{ll_1l_2}\{l(l+1)[l(l+1) + l_1(l_1+1) - l_2(l_2+1)]\} b_l b_{l_1} b_{l_2}. \tag{42}$$

Notice that these expressions are generic, in that they are derived without any specific assumption about the shape of the bispectrum. The rest of the terms can be expressed in terms of the power spectrum alone. As is common practice in the literature these results ignore all higher-order correlation beyond the bispectrum.

$$S_l^{\langle\Theta^2,\nabla\Theta\cdot\nabla\Theta\rangle}(\theta_b) = \frac{1}{2l+1}\sum_{l_i=2}^{l_{\rm max}} \begin{pmatrix} l_1 & l_2 & l \\ 0 & 0 & 0 \end{pmatrix}^2 I^2_{l_1l_2l}[l(l+1) + l_1(l_1+1) - l_2(l_2+1)](\mathcal{C}_{l_1} b_{l_1}^2 + n_{l_1})(\mathcal{C}_{l_2} b_{l_2}^2 + n_{l_2}), \tag{43}$$

$$S_l^{\langle\Theta^2,\Theta^2\rangle} = \frac{2}{2l+1}\sum_{l_i=2}^{l_{\rm max}} \begin{pmatrix} l_1 & l_2 & l \\ 0 & 0 & 0 \end{pmatrix}^2 I^2_{l_1 l_2 l}(\mathcal{C}_{l_1} b^2_{l_1} + n_{l_1})(\mathcal{C}_{l_2} b^2_{l_2} + n_{l_2}), \tag{44}$$

$$S_l^{\langle\nabla\Theta\cdot\nabla\Theta,\nabla\Theta\cdot\nabla\Theta\rangle} = \frac{2}{2l+1}\sum_{l_i=2}^{l_{\rm max}} \begin{pmatrix} l_1 & l_2 & l \\ 0 & 0 & 0 \end{pmatrix}^2 I^2_{l_1 l_2 l}[l(l+1)+l_1(l_1+1)-l_2(l_2+1)]^2(\mathcal{C}_{l_1} b^2_{l_1} + n_{l_1})(\mathcal{C}_{l_2} b^2_{l_2} + n_{l_2}). \tag{45}$$

The remaining terms are scaled input power-spectra:

$$S_l^{\langle\Theta,\nabla^2\Theta\rangle} = -l(l+1)(\mathcal{C}_l b_l^2 + n_l); \quad S_l^{\langle\nabla^2\Theta,\nabla^2\Theta\rangle} = l^2(l+1)^2(\mathcal{C}_l b_l^2 + n_l); \quad S_l^{\Theta,\Theta} = (\mathcal{C}_l b_l^2 + n_l). \tag{46}$$

The derivation of these results follows the same general principle that is outlined in Section 5. These expressions are used to compute the cross-correlation coefficient among various spectra which are defined below:

$$r_l^{ij}(\theta_b) = \left\langle \delta S_l^{(i)}(\theta_b)\delta S_l^{(j)}(\theta_b)\right\rangle / \sqrt{\left\langle [\delta S_l^{(i)}(\theta_b)]^2\right\rangle}\sqrt{\left\langle [\delta S_l^{(j)}(\theta_b)]^2\right\rangle}; \qquad i,\, j \in \{0,1,2\}. \tag{47}$$

As before, throughout we have ignored the mode–mode coupling. The coefficients of cross-correlation r_{ij} are independent of the sky-coverage $f_{\rm sky}$. The S/N for individual modes for a given spectrum on the other hand can be expressed as

$$[S/N]_l^{(i)}(\theta_b) = \sqrt{\langle [S_l^{(i)}(\theta_b)]^2\rangle / \langle [\delta S_l^{(i)}(\theta_b)]^2\rangle} \qquad i \in \{0,1,2\}. \tag{48}$$

The cumulative $[{\rm S/N}] = \sum_{l=2}^{l_{\rm max}} [{\rm S/N}]_l^{(i)}$ is tabulated for individual experiments in Table 2 for *Planck* and *EPIC*.

We have also computed the S/N for individual modes using these expressions for various skew-spectra. These results are plotted in Fig. 8 for *Planck* as well as for *EPIC* in Fig. 9. The cumulative S/N as expected is higher for *EPIC* due to higher sensitivity. The S/N for ISW decreases sharply at higher l and peaks at lower l; on the other hand the S/N for SZ and unresolved PSs peaks at a much higher angular frequency. Among the three skew-spectra we have considered, the skew-spectra $S_l^{(1)}(\theta_b)$ was found to have a higher S/N compared to $S_l^{(0)}(\theta_b)$ and $S_l^{(2)}(\theta_b)$. While the lowest order skew-spectra $S_l^{(0)}(\theta_b)$ is dominated mostly by cosmic variance the other skew-spectra, $S_l^{(2)}(\theta_b)$, is maximally affected by the instrumental noise. The information content is not independent for the different skew-spectra; their cross-correlation coefficient provides a succinct measure of this lack of dependence. The cross-correlation coefficients for *Planck* are plotted in Fig. 10 and for *EPIC* in Fig. 11. For *Planck* the coefficients are noise dominated and are same for all three-types of skew-spectra considered. For *EPIC*, the level of noise is low which leads to a tight correlation among various estimators.

Table 2. The cumulative S/N for *Planck* and *EPIC* surveys are shown for the three one-point skew-spectra. Parameters used to compute the skew-spectra and the associated scatter for the two different experiments, ongoing *Planck* (Planck Collaboration 2008) and *EPIC* (Baumann et al. 2009).

(*Planck*,*EPIC*)	SZ	ISW	PS
S/N	(5.0, 1137.4)	(1.0, 216.0)	(0.5, 209.0)
S/N	(24.0, 1354.9)	(62.2, 420.3)	(4.3, 552.0)
S/N	(19.7, 1328.8)	(31.8, 246.5)	(1.7, 421.0)

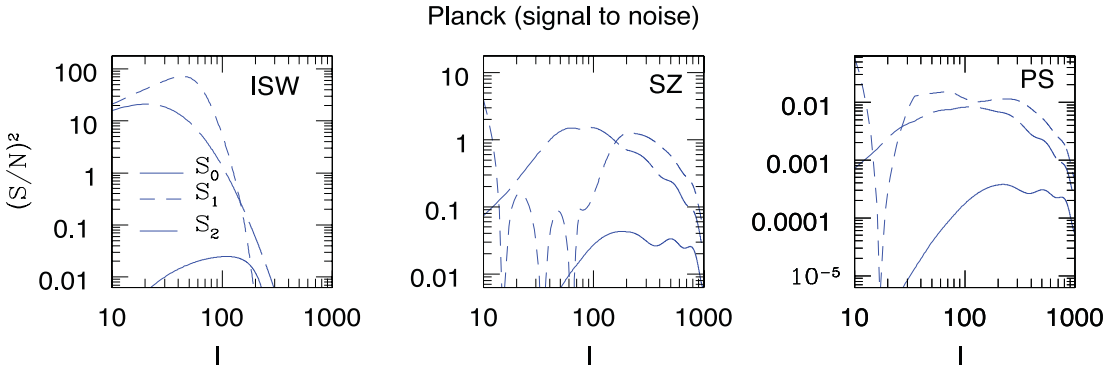

Figure 8. The mode-by-mode S/N is depicted for the three skew-spectra, ISW (left-hand panel), SZ (middle-panel) and PS (right-hand panel), as a function of the harmonics l. In each panel solid, short-dashed and long-dashed lines correspond to $S_0(\theta_b)$, $S_1(\theta_b)$ and $S_2(\theta_b)$, respectively. The specific experimental set-up considered here is that of ongoing experiment *Planck* (143 GHz frequency channel). The parameters defining this experiment are summarized in Table 1. We have assumed an all-sky coverage $f_{\rm sky} = 1$. The mixed bispectrum that the skew-spectra sample corresponds to cross-correlation of lensing and thermal SZ effect. All other source of primordial non-Gaussianity has been ignored. We use equation (29) in conjunction with equation (31) in our computation of the scatter.

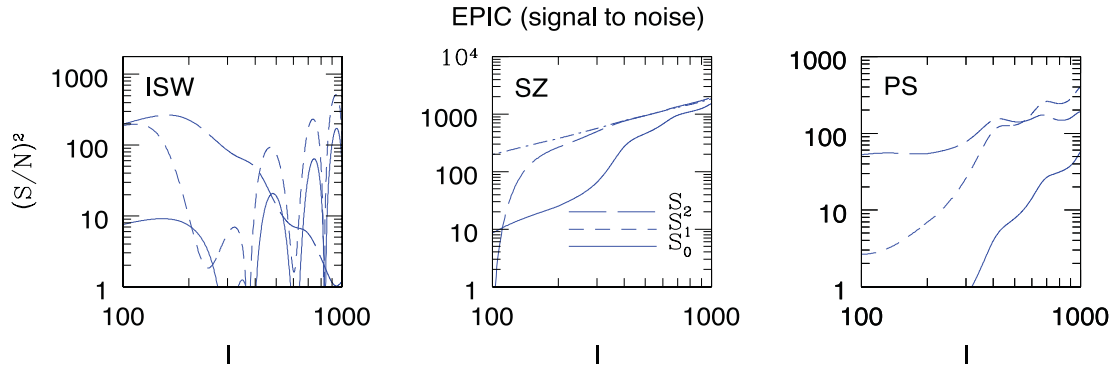

Figure 9. Same as previous figure but for the *EPIC* experiment (150 GHz frequency channel; see Table 1 for the parameters defining this experiment).

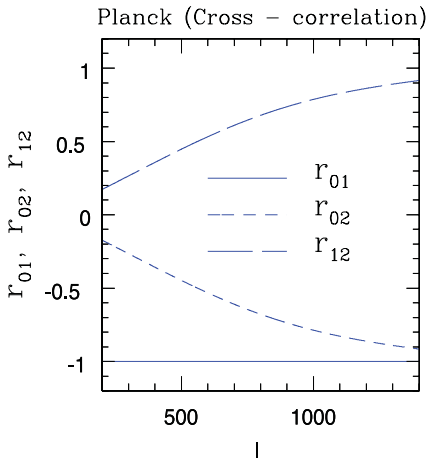

Figure 10. The information content of the skew-spectra is not completely independent. The level of cross-correlation among various estimators is encoded in the coefficient of cross-correlations r_{ij} defined in equation (47). The cross-correlation coefficients r_{01}, r_{02} and r_{12} are plotted as a function of harmonics l. The noise level corresponds to that of *Planck* (see Table 1). The correlation structure reflects the underlying spectra β_l as well as the level of noise. The expression for scatter equations (34)–(36) and cross-correlation equations (37)–(39) have two contributions. In each of these expressions there are terms which depend on the bispectrum and there are terms which can be constructed from power spectrum alone. For *Planck*, we found that the expressions for the scatter as well as the cross-correlation are entirely dominated by the terms which depend only on the power spectrum, thus making the coefficient r_{ij} independent of the type of underlying bispectrum.

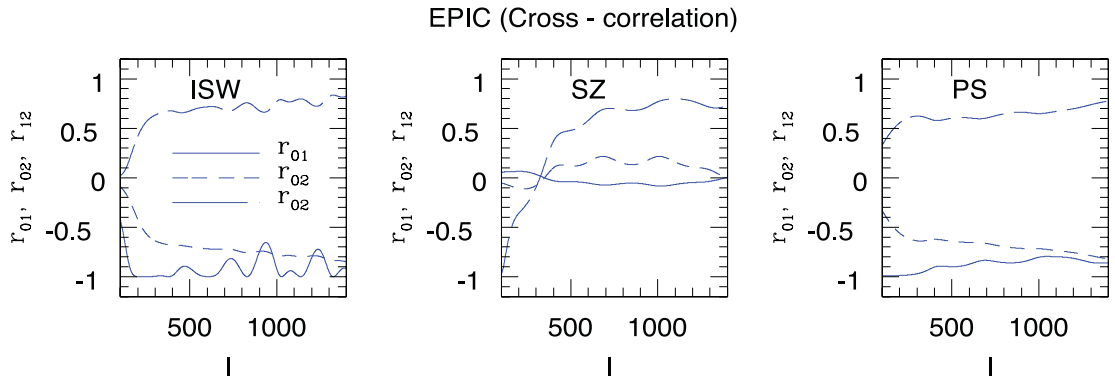

Figure 11. Same as previous figure but for *EPIC* experiment (see Table 1). However for *EPIC* the expressions for scatter and cross-correlation are not completely dominated by noise. The left-hand, middle and right-hand panels correspond to ISW, SZ and PS skew-spectra.

To correct for the effect of a mask and the noise we will follow the PCL method devised by Hivon et al. (2002) for the power spectrum analysis and later developed by Munshi et al. (2011c) for analysing the skew-spectra and the kurt-spectrum (Munshi et al. 2011b) and the cross-correlation coefficient provides a valuable indicator of their independence.

The S/N of estimates of one-point generalized skewness parameters $S^{(i)} = \sum_{l=2}^{l_{\rm max}} (2l+1) S_l^{(i)}$ is given by $[\sum_{l=2}^{l_{\rm max}} (2l+1)^2 \langle [\delta S^{(i)}/S^{(i)}]^2 \rangle]^{-1/2}$. The corresponding numbers for *Planck* and *EPIC* are presented in Table 3. It is possible to introduce a filter function $w_{l_1 l_2}$ in the definition of the skew-spectra. Choices include sharp cutoff in the l space to avoid the effect of noise

Table 3. The cumulative S/N for *Planck* and *EPIC* surveys for the one-point cumulants $S^{(i)}(\hat{\Omega})$, defined in equation (48), are shown for each skew-spectra. Parameters used to compute the skew-spectra and the associated scatter for the two different experiments, ongoing *Planck* (Planck Collaboration 2008) and *EPIC* (Baumann et al. 2009). We have assumed $f_{\rm sky} = 1$ in our calculations.

Planck,*EPIC*	SZ	ISW	PS
S/N	(3.8, 503.2)	(0.3, 39.3)	(0.4, 53.4)
S/N	(5.8, 1299.0)	$(6.4 \times 10^{-2}, 70.9)$	(0.6, 529.1)
S/N	(1.2, 625.8)	$(1.4 \times 10^{-2}, 21.1)$	(0.1, 178.2)

at high l to optimal filters that maximize the S/N for a given resolution $l_{\rm max}$. Clearly, such option will invariably improve the statistical significance. The filter functions can be of further interest if the bispectrum is more pronounced for certain triangular configurations. Another potentially useful application of a filter function is to filter out a specific configuration. However, in such a case the skew-spectra will not have any direct relation with the topological properties of the original map.

7 CONCLUSION AND DISCUSSION

Non-Gaussianity is in itself a poorly defined concept. In it there is no unique approach that can be adopted to describe or parametrize an arbitrary form of non-Gaussianity in a complete manner. In order to quantify non-Gaussianity as fully as possible it is therefore essential to deploy a battery of complementary approaches, each of which exploits different statistical characteristics. Each such technique will have a unique response to real world issues such as the sky-coverage (observational mask), beam and instrumental noise. Any robust detection therefore will have to involve a simultaneous cross-validation of results obtained from independent methods. The most common characterizations of non-Gaussianity involve studying the bispectrum, which represents the lowest-order departure from Gaussianity; higher-order non-Gaussianity can be studied using its higher-order analogues, i.e. the multi-spectra.

In contrast, the topological estimators (MFs) that we have studied here carry information to all orders, though in a collapsed (one-point) form. Analytical results for MFs for a Gaussian field are well understood, and form the basis of non-Gaussianity studies (Tomita 1986). There have been several previous studies on extraction of the MFs from the CMB data that rely either on simplification of radiative transfer using the Sachs–Wolfe limit (Hikage et al. 2006) or using a perturbative approach based on a series expansion of the MFs that can be studied order by order (Matsubara 2003b, 1994). The MFs have also been studied using elaborate computer-intensive non-Gaussian simulations (Komatsu et al. 2003; Spergel et al. 2007). Most of these studies were done using a specific model of non-Gaussianity, namely the *local* model of primordial non-Gaussianity which is parametrized by the well-known parameter $f_{\rm NL}$.

The main motivation behind the present study has been to extend such methods to secondary non-Gaussianities which have not been studied before in the context of morphological statistics analytically. The increase in sensitivity of CMB experiments and near all-sky coverage along with wide frequency range mean the study of non-Gaussianities will be feasible in the very near future. Moreover, in the currently favoured adiabatic CDM models it is expected that the contribution from primordial non-Gaussianity is negligible and the main contribution to non-Gaussianities comes from secondaries. The secondary non-Gaussianity signals are associated with large-scale structure contributions and through various mode coupling effects such as gravitational lensing (Goldberg & Spergel 1999a,b; Cooray & Hu 2000). Our primary aim in this work has been to study how well we can probe the secondary signals from mode coupling using morphological descriptors.

One of the main difficulties faced by one-point estimators $S^{(i)}(\theta_b)$, which also affects the MF-based estimators $V_k(\nu)$, is their inability to differentiate among various sources of non-Gaussianity. The triplets of skew-spectra $S_l^{(i)}(\theta_b)$ that we have introduced can be used to separate out contributions from various secondaries as well as to probe and constrain any foreground residuals left from the component separation step of the data analysis chain. Generalizing Munshi & Heavens (2010) we have introduced a set of triplets of skew-spectra which can be extracted from any realistic data. These skew-spectra do not compress the available information from a bispectrum to a single number, and their shape can help to distinguish among various sources of non-Gaussianity. Exploiting the perturbative expansion of the MFs, we showed that at the leading order of non-Gaussianity the MFs are completely specified by the knowledge of the bispectrum. Our results are most naturally defined in the harmonic domain. Comparison of MFs extracted using harmonic approach can be cross-compared with more traditional approach in the real space as a useful consistency check.

The methods based on the skew-spectra that we have presented are simple to implement once the derivative fields $[\nabla\Theta \cdot \nabla\Theta]$ or $[\nabla^2\Theta]$ are constructed. We have shown that this can be implemented in a model-independent way. Our method is based on a PCL approach (Hivon et al. 2002) and can handle arbitrary sky coverage and inhomogeneous noise distributions. The PCL approach is well understood in the context of power spectrum studies, and its variance or scatter can be computed analytically. We provide generic analytical results for the computation of scatter around individual estimates. We also provide detailed predictions on how they are cross-correlated. In our method, it is possible indeed to go beyond the lowest level in non-Gaussianity to include the contribution from trispectrum. The main contributions in frequency-cleaned CMB maps will be from lensing of the CMB, though it is expected that such corrections will be sub-dominant at least in the context of CMB data analysis.

We conclude by pointing out that the MFs do not probe the full bispectrum, but involve only weighted sums of modes and are thus equivalent to the three *generalized* skewness parameters we have used. We have also defined three generalized skew-spectra associated with each of these skewness parameters. In this sense, the study of these skew-spectra can replace the study of MFs. The skew-spectra we have introduced can all be probed for arbitrary mask and noise. Unbiased estimators can also be constructed which can work in the presence of partial sky coverage and inhomogeneous noise. Their variance can also be computed *analytically*; thereby avoiding the use of non-Gaussian Monte Carlo simulations completely. Finally, the MFs can be constructed from the knowledge of generalized skew-spectra and can be compared with the results from real space analysis. The triplets of generalized skew-spectra can be used to separate individual components of NGs using their shape information. From our analytical results of cross-correlation, we find that in the absence of noise, e.g. experiments such as *EPIC*, the skew-spectra are highly correlated, more so for higher l values. The correlation coefficients are typically in the range $r = 0.5$–1 for a *Planck*-type experiment. The cumulative S/N, in a *Planck*-type experiment, for bispectrum corresponding to the ISW and SZ and lensing cross-correlation reaches $\mathcal{O}(10)$. An improvement of about two orders of magnitude can be expected with experiments such as *EPIC*.

Throughout we have ignored the presence of primordial non-Gaussianity which is expected to be subdominant. Nevertheless, it can be incorporated. Individual skew-spectra from different underlying bispectrum can essentially be combined to construct the total skew-spectra which means that our results can straightforwardly be generalized to incorporate specific models of primordial non-Gaussianity.

The generic results derived here are also applicable to other areas in cosmology and have indeed been explored recently. Examples include the analysis of galactic redshift surveys (Pratten & Munshi 2012), weak lensing surveys (Munshi et al. 2012b) and the frequency-cleaned SZ maps (Munshi et al. 2012a). The results presented here can be extended beyond the analysis of temperature maps, e.g. to analyse polarization maps, by extending the spin-0 calculations to spin-2. Such results can furnish useful probes for the characterization of morphology of reionization in three dimensions.

A few comments are in order about the comparison of our estimators with the so-called optimal estimators. The motivation to construct an optimal estimator is to improve the S/N of detection which is important in case of weak signals such as the primordial non-Gaussianity. The main motivation in this paper has been to reconstruct the topological properties of the CMB map going beyond Gaussianity, in the harmonic domain, in particular due to the contributions from secondary-lensing cross-correlation which will be detected with high S/N with the proposed CMB surveys such as *EPIC*.

In addition to the primary and secondary non-Gaussianity, cosmic defects such as textures or cosmic strings (Albrecht, Battey & Robinson 1999; Cruz et al. 2007; Regan & Shellard 2010) also leave non-Gaussian footprints in CMB maps which can be detected by the change in topological nature of the maps. The estimators we have presented here may have relevance in such investigations. A detailed study will be presented elsewhere.

At the level of the bispectrum the effect of lensing can only be studied through its cross-correlation with other secondaries. However weak lensing is also independently responsible for a next order correction to MFs through its effect on the trispectrum; the S/N is expected to be low.

The S/N of the skew-spectra for secondary-lensing cross-correlation bispectrum is comparable to that of the skew-spectra of frequency-cleaned SZ maps (Munshi et al. 2012a). However, the secondary skew-spectra are much higher compared to skew-spectra associated with primary skew-spectra unless we assume a rather high value for the $f_{\rm NL}$.

ACKNOWLEDGMENTS

DM and PC acknowledge support from STFC standard grant ST/G002231/1 at the School of Physics and Astronomy at Cardiff University where this work was completed. DM would like to thank Joseph Smidt, Geraint Pratten, Asantha Cooray, Shahab Joudaki and Erminia Calabrese for very useful discussions.

REFERENCES

Acquaviva V., Bartolo N., Matarrese S., Riotto A., 2003, Nucl. Phys. B, 667, 119
Adler R. J., 1981, The Geometry of Random Fields. Wiley, Chichester
Albrecht A., Battye R. A., Robinson J., 1999, Phys. Rev. D., 59, 023508
Babich D., 2005, Phys. Rev. D, 72, 043003
Bartolo N., Komatsu E., Matarrese S., Riotto A., 2004, Phys. Rep., 402, 103
Bartolo N., Matarrese S., Riotto A., 2006, J. Cosmol. Astropart. Phys., 06, 024
Baumann D. et al., 2009, AIP Conf. Proc. Vol. 1141, CMB Polarization Workshop: Theory and Foregrounds. Am. Inst. Phys., New York, p. 10 (arXiv:0811.3919)
Birkinshaw M., 1999, Phys. Rep., 310, 97
Bock J. et al., 2008, preprint (arXiv:0805.4207)
Bock J. et al., 2009, preprint (arXiv:0906.1188)
Boughn S., Crittenden R., 2004, Nat, 427, 45
Calabrese E., Smidt J., Amblard A., Cooray A., Melchiorri A., Serra P., Heavens A., Munshi D., 2010, Phys. Rev. D., 81, 3529
Canavezes A. et al., 1998, MNRAS, 297, 777
Castro P. G., 2004, Phys. Rev. D, 67, 044039
Chen X., 2010, Adv. Astron., 2010, id 638979
Coles P., 1988, MNRAS, 234, 509
Cooray A, Sheth R., 2002, Phys. Rep., 372, 1

Cooray A., 2001a, Phys. Rev. D, 64, 043516
Cooray A., 2001b, Phys. Rev. D, 64, 063514
Cooray A., 2002, Phys. Rev. D, 65, 103510
Cooray A., 2006, Phys. Rev. Lett., 97, 261301
Cooray A. R., Hu W., 2000, ApJ, 534, 533
Cooray A., Kesden M., 2003, New Astron., 8, 231
Cooray A., Li C., Melchiorri A., 2008, Phys. Rev. D, 77, 103506
Copi C., Huterer D., Schwarz D., Starkman G., 2007, Phys. Rev. D, 75, 023507
Cruz M., Turok N., Vielva P., Martinez-Gonzaléz E., Hobson M., 2007, Sci, 318, 1612
Das S. et al., 2011, Phys. Rev. Lett., 107, 021301
Edmonds A. R., 1968, Angular Momentum in Quantum Mechanics, 2nd edn. rev. printing. Princeton Univ. Press, Princeton, NJ
Falk T., Madden R., Olive K. A., Srednicki M., 1993, Phys. Lett. B, 318, 354
Ferreira P. G., Magueijo J., Gorski K. M., 1998, ApJ, 503, 1
Gangui A., Lucchin F., Matarrese S., Mollerach S., 1994, ApJ, 430, 447
Gleser L., Nusser A., Ciardi B., Desjacques V., 2006, MNRAS, 370, 1329
Goldberg D. M., Spergel D. N., 1999a, Phys. Rev. D, 59, 103001
Goldberg D. M., Spergel D. N., 1999b, Phys. Rev. D, 59, 103002
Gott J. R., Mellot A. L., Dickinson M., 1986, ApJ, 306, 341
Gott J. R. et al., 1989, ApJ, 340, 625
Gott J. R., Park C., Juszkiewicz R., Bies W. E., Bennett D. P., Bouchet F. R., Albert S., 1990, ApJ, 352, 1
Gott J. R., Mao S., Park C., Lahav O., 1992, ApJ, 385, 26
Hadwiger H., 1959, Math Z., 71, 124
Hanson F. K., Lewis A., 2009, Phys. Rev. D, 80, 063004
Hikage C. et al., 2002, Publ. Astron. Soc. Jap., 54, 707
Hikage C., Komatsu E., Matsubara T., 2006, ApJ, 653, 11
Hikage C., Coles P., Grossi M., Moscardini L., Dolag K., Branchini E., Matarrese S., 2008a, MNRAS, 385, 1613
Hikage C., Matsubara T., Coles P., Liguori M., Hansen F. K., Matarrese S., 2008b, MNRAS, 389, 1439
Hinsaw G., Banday A. J., Bennett C. L., Gorski K. M., Kogut A., 1995, ApJ, 446, 67
Hivon E., Górski K. M., Netterfield C. B., Crill B. P., Prunet S., Hansen F., 2002, ApJ, 567, 2
Hoftuft J., Eriksen H. K., Banday A. J., Gorski K. M., Hansen F. K., Lilje P. B., 2009, ApJ, 699, 985
Hu W., Scott D., Silk J., 1994, Phys. Rev. D, 49, 648
Joudaki S., Smidt J., Amblard A., Cooray A., 2010, J. Cosmol. Astropart. Phys., 08, 027
Kaminkowski M., Spergel D., 1994, ApJ, 432, 7
Kamionkowski M., Smith T. L., Heavens A., 2011, Phys. Rev. D, 83, 023007
Kerscher M., Mecke K., Schmalzing J., Beisbart C., Buchert T., Wagner H., 2001, A&A., 373, 1
Kofman L. A., Starobinsky, 1985, Sov. Astron. Lett., 11, 271
Komatsu E. et al., 2003, ApJS, 148, 119
Larson D. et al., 2011, ApJS, 192, 16
Luminet J. P., Weeks J., Riazuelo A., Lehoucq R., Uzan J. P., 2003, Nat, 425, 593
Maldacena J. M., 2003, J. High Energy Phys., 05, 013
Martinez-Gonzaléz E., Sanz J.-L, Silk J., 1990, ApJ, 355, L5
Matsubara T., 1994, ApJ, 434, L43
Matsubara T., 1995, ApJS, 101, 1
Matsubara T., 2003a, ApJ, 584, 1
Matsubara T., 2003b, ApJ, 584, 1
Matsubara T., Jain B., 2001, ApJ, 552, L89
Matsubara T., Yokohama J., 1996, ApJ, 463
Melott A. L., 1990, Phys. Rep., 193, 1
Mollerach S., Gangui A., Lucchin F., Mataresse S., 1995, ApJ, 453, 1
Moore B. et al., 1992, MNRAS, 256, 477
Mukhanov V. F., Feldman H. A., Bandenberger R. H., 1992, Phys. Rev. D, 215, 203
Munshi D., Heavens A., 2010, MNRAS, 401, 2406
Munshi D., Souradeep T., Starobinsky, 1995, ApJ, 454, 552
Munshi D., Melott A. L., Coles P., 2000, MNRAS, 311, 149
Munshi D., Heavens A., Cooray A., Smidt J., Coles P., Serra P., 2011c, MNRAS, 412, 1993
Munshi D., Coles P., Cooray A., Heavens A., Smidt J., 2011a, MNRAS, 410, 1295
Munshi D., Smidt J., Heavens A., Coles P., Cooray A., 2011b, MNRAS, 411, 2241
Munshi D., Valageas P., Cooray A., Heavens A., 2011c, MNRAS, 414, 3173
Munshi D., Kitching T., Heavens A., Coles P., 2011d, MNRAS, 416, 629
Munshi D., Smidt J., Cooray A., 2010, preprint (arXiv:1011.5224)
Munshi D., Smidt J., Joudaki S., Coles P., 2012a, MNRAS, 419, 138
Munshi D., van Waerbeke L., Smidt J., Coles P., 2012b, MNRAS, 419, 536
Natoli P. et al., 2010, MNRAS, 408, 1658
Novikov D., Schmalzing J., Mukhanov V. F., 2000, A&A, 364
Park C. et al., 2005, ApJ, 633, 11
Pratten G., Munshi D., 2012, MNRAS, 423, 3209
Regan D. M., Shellard E. P. S., 2010, Phys. Rev. D, 82, 063527
Roukemia B. F., Lew B., Cechowska M., Marecki A., Bajtlik S., 2004, A&A, 423, 821

Sahni V., Sathyaprakash B. S., Shandarin S. F., 1998, ApJ, 495, L5
Salopek D. S., Bond J. R., 1990, Phys. Rev. D, 42, 3936
Salopek D. S., Bond J. R., 1991, Phys. Rev. D, 43, 1005
Sato J., Takada M., Jing Y. P., Futamase T., 2001, ApJ, 551, 5
Schmalzing J., Diaferio A., 2000, MNRAS, 312, 638
Schmalzing J., Górski K. M., 1998, MNRAS, 297, 355
Smidt J., Joudaki S., Serra P., Amblard A., Cooray A., 2010, Phys. Rev. D, 81, 123528
Smith K. M., Zahn O., Dore O., 2007, Phys. Rev. D, 76, 043510
Spergel D. N. et al., 2007, ApJS, 170, 377
Szapudi I., Szalay A. S., 1999, ApJ, 515, L43
Taruya A., Takada M, Hamana T., Kayo I., Futamase T., 2002, ApJ, 571, 638
The COrE Collaboration, 2012, preprint (2011arXiv1102.2181)
Tomita H., 1986, Progr. Theor. Phys., 76, 952
van Engelen A. et al., 2012, ApJ, 756, 142
Verde L., Spergel D. N., 2002, Phys. Rev. D., 65, 043007

APPENDIX A: SPHERICAL HARMONICS

The completeness relationship for the spherical harmonics $Y_{lm}(\hat{\Omega})$ is given by

$$\sum_{lm} Y_{lm}(\hat{\Omega}) Y^*_{lm}(\hat{\Omega}') = \delta_{2\mathrm{D}}(\hat{\Omega} - \hat{\Omega}'). \tag{A1}$$

The orthogonality relationship is as follows:

$$\int \mathrm{d}\hat{\Omega}\; Y_{lm}(\hat{\Omega}) Y^*_{l'm'}(\hat{\Omega}) = \delta^{\mathrm{K}}_{ll'} \delta^{\mathrm{K}}_{mm'}. \tag{A2}$$

Here $\delta_{2\mathrm{D}}$ and δ^{K} represent the Dirac's 2D delta function and Kroneker's Delta function, respectively.

APPENDIX B: 3J SYMBOLS

The following properties of 3*j* symbols were used to simplify various expressions.

$$\sum_{l_3 m_3} (2l_3 + 1) \begin{pmatrix} l_1 & l_2 & l_3 \\ m_1 & m_2 & m_3 \end{pmatrix} \begin{pmatrix} l_1 & l_2 & l \\ m'_1 & m'_2 & m \end{pmatrix} = \delta^K_{m_1 m'_1} \delta^K_{m_2 m'_2}; \tag{B1}$$

$$\sum_{m_1 m_2} \begin{pmatrix} l_1 & l_2 & l_3 \\ m_1 & m_2 & m_3 \end{pmatrix} \begin{pmatrix} l_1 & l_2 & l'_3 \\ m_1 & m_2 & m'_3 \end{pmatrix} = \frac{\delta^K_{l_3 l'_3} \delta^K_{m_3 m'_3}}{2l_3 + 1}; \tag{B2}$$

$$(-1)^m \begin{pmatrix} l & l & l' \\ m & -m & 0 \end{pmatrix} = \frac{(-1)^l}{\sqrt{(2l+1)}} \delta^K_{l'0}; \tag{B3}$$

$$\int d\hat{\Omega} Y_{lm}(\hat{\Omega}) Y_{l'm'}(\hat{\Omega}) Y_{LM}(\hat{\Omega}) = \sqrt{\frac{(2l+1)(2l+1)(2L+1)}{4\pi}} \begin{pmatrix} l & l' & L \\ m & m' & M \end{pmatrix} \begin{pmatrix} l & l' & L \\ 0 & 0 & 0 \end{pmatrix}. \tag{B4}$$

This paper has been typeset from a TEX/LATEX file prepared by the author.